UPPSALA
UNIVERSITET

Digital Comprehensive Summaries of Uppsala Dissertations from the Faculty of Science and Technology 237

Tuning of the Excited State Properties of Ruthenium(II)-Polypyridyl Complexes

MARIA ABRAHAMSSON

ACTA
UNIVERSITATIS
UPSALIENSIS
UPPSALA
2006

ISSN 1651-6214
ISBN 91-554-6707-5
urn:nbn:se:uu:diva-7230

Dissertation presented at Uppsala University to be publicly examined in Häggsalen, Ångströmlaboratoriet, Lägerhyddsvägen 1, Uppsala, Friday, December 1, 2006 at 09:30 for the degree of Doctor of Philosophy. The examination will be conducted in English.

Abstract
Abrahamsson, M. 2006. Tuning of the Excited State Properties of Ruthenium(II)-Polypyridyl Complexes. Acta Universitatis Upsaliensis. *Digital Comprehensive Summaries of Uppsala Dissertations from the Faculty of Science and Technology* 237. 79 pp. Uppsala.
ISBN 91-554-6707-5.

Processes where a molecule absorbs visible light and then converts the solar energy into chemical energy are important in many biological systems, such as photosynthesis and also in many technical applications e.g. photovoltaics. This thesis describes a part of a multidisciplinary project, aiming at a functional mimic of the natural photosynthesis, with the overall goal of production of a renewable fuel from sun and water. More specific, the thesis is focused on design and photophysical characterization of new photosensitizers, i.e. light absorbers that should be capable of transferring electrons to an acceptor and be suitable building blocks for supramolecular rod-like donor-photosensitizer-acceptor arrays.

The excited state lifetime, the excited state energy and the geometry are important properties for a photosensitizer. The work presented here describes a new strategy to obtain longer excited state lifetimes of the geometrically favorable Ru(II)-bistridentate type complexes, without a concomitant substantial decrease in excited state energy. The basic idea is that a more octahedral coordination around the Ru will lead to longer excited state lifetimes. In the first generation of new photosensitizers a 50-fold increase of the excited state lifetime was observed, going from 0.25 ns for the model complex to 15 ns for the best photosensitizer. The second generation goes another step forward, to an excited state lifetime of 810 ns. Furthermore, the third generation of new photosensitizers show excited state lifetimes in the 0.45 - 5.5 microsecond region at room temperature, a significant improvement. In addition, the third generation of photosensitizers are suitable for further symmetric attachment of electron donor and acceptor motifs, and it is shown that the favorable properties are maintained upon the attachment of anchoring groups. The reactivity of the excited state towards light-induced reactions is proved and the photostability is sufficient so the new design strategy has proven successful.

Keywords: Artificial photosynthesis, Ruthenium(II), Bistridentate complexes, Excited state lifetime, Linear donor-photosenstizer-acceptor arrays, Temperature dependence, Excited state decay

Maria Abrahamsson, Department of Photo Chemistry and Molecular Science, Box 523, Uppsala University, SE-75120 Uppsala

ISSN 1651-6214
ISBN 91-554-6707-5
urn:nbn:se:uu:diva-7230 (http://urn.kb.se/resolve?urn=urn:nbn:se:uu:diva-7230)

Till mormor

"Nothing in life is to be feared, it is only to be understood."

Marie Curie

List of Papers

This thesis is based on the following papers, and will be referred to in the text by their Roman numerals.

I. **A Tridentate Ligand for Preparation of Bisterpyridine-like Ruthenium(II) Complexes with an Increased Excited State Lifetime**
H. Wolpher, O. Johansson, M. Abrahamsson, M. Kritikos, L. Sun, B. Åkermark
Inorganic Chemistry Communications, **2004**, *7*, 337-340

II. **A New Strategy for the Improvement of Photophysical Properties in Ruthenium(II) Polypyridyl Complexes. Synthesis and Photophysical and Electrochemical Characterization of Six Mononuclear Ruthenium(II) Bisterpyridine-Type Complexes**
M. Abrahamsson, H. Wolpher, O. Johansson, J. Larsson, M. Kritikos, L. Eriksson, P.-O. Norrby, J. Bergquist, L. Sun, B. Åkermark, L. Hammarström
Inorganic Chemistry, **2005**, *44*, 3215-3225

III. **Steric Influence on the Excited Styte Lifetimes of Ruthenium complexes with Bipyridyl-Alkanylene-Pyridyl Ligands**
M. J. Lundqvist, P. Persson, M. Abrahamsson, H.-C. Becker, L. Hammarström, H. Wolpher, O. Johansson, B. Åkermark, L. Eriksson, J. Bergquist, P.-O. Norrby
Manuscript

IV. **Six-Membered Ring Chelate Complexes of Ru(II): Structural and Photophysical Effects**
M. Abrahamsson, H.-C. Becker, L. Hammarström, C. Bonnefous, C. Chamchoumis, R. P. Thummel
Manuscript

V. **A 3.0 μs Room Temperature Excited State Lifetime of a Bistridentate RuII-Polypyridine Complex for Rod-like Molecular Arrays**
M. Abrahamsson, M. Jäger, T. Österman, L. Eriksson, P. Persson, H.-C. Becker, O. Johansson, L. Hammarström
Journal of American Chemical Society, **2006**, *128*, 12616-12617

VI. **Bistridentate Ru(II)-Polypyridyl Complexes with Microsecond MLCT Excited State Lifetimes: Synthesis and Photophysical Properties**
M. Abrahamsson, M. Jäger, T. Österman, P. Persson, H.-C. Becker, O. Johansson, L. Hammarström
Manuscript

VII. **Modulation of the Lowest MLCT State in $[Ru(bpy)_2(N\text{-}N)]^{2+}$ Systems by Changing the N-N from Hydrazone to Azine. Photophysical Consequences**
M. Abrahamsson, L. Hammarström, D. A. Tocher, S. Nag, D. Datta
Inorganic Chemistry, Published on the Web 2006-10-18

VIII. **Structural and Spectral Investigation of Ruthenium(II) Polypyridyl Complexes by DFT calculations**
M. J. Lundqvist, O. A. Borg, M. Abrahamsson, B. Åkermark, S. Lunell, P. Persson
Submitted to Inorganic Chemistry

Papers related to but not included in this thesis

IX. **Synthesis and Characterization of Dinuclear Ruthenium Complexes Covalently Linked to RuII Tris-bipyridine: An Approach to Mimics of the Donor Side of Photosystem II**
Y. Xu, G. Eilers, M. Borgström, J. Pan, M. Abrahamsson, A. Magnuson, R. Lomoth, J. Bergquist, T. Polívka, L. Sun, V. Sundström, S. Styring, L. Hammarström, B. Åkermark
Chemistry - A European Journal, **2005**, *11*, 7305-7314

X. **Bio-Inspired, Side-on Attachment of a Ruthenium Photosensitizer to an Iron Hydrogenase Active Site Model**
J. Ekström, M. Abrahamsson, C. Olson, J. Bergquist, F. B. Kaynak, L. Eriksson, L. Sun, H.-C. Becker, B. Åkermark, L. Hammarström, S. Ott
Dalton Transactions **2006**, 4599-4606

Comments on my participation

I am responsible for all the photophysical work in papers I-VII, the photochemical work in paper VI, the spectroelectrochemistry in paper VII and the electrochemistry in paper IV. I contributed to the writing of all papers and carried the main responsibility for the writing of paper II, V, VI, and VII and shared the writing responsibility for paper III and IV. Paper VIII is a result of a collaboration between experimentalists and computational chemists, and my main contribution is to the discussion. In paper IX I carried out some of the photophysical characterization, and I was responsible for the photophysical measurements and contributed to the writing of paper X.

Contents

Abbreviations

A	electron acceptor
B3LYP	three-parameter hybrid functional
bpy	2,2´-bipyridine
bpyz	bipyrazine
D	electron donor
DFT	density functional theory
dppz	dipyrido[3,2-a:2',3'-c]phenazine
EnT	energy transfer
ET	electron transfer
HOMO	highest occupied molecular orbital
IC	internal conversion
ISC	intersystem crossing
LC	ligand-centered
LMCT	ligand-to-metal charge transfer
MC	metal-centered
MLCT	metal-to-ligand charge transfer
MM	molecular mechanics
ns	nanosecond
P	photosensitizer
ps	picosecond
PS I	photosystem I
PS II	photosystem II
py	pyridine
TD-DFT	time-dependent DFT
tpy	2,2´:6´,2´´-terpyridine
ttpy	4´-tolyl-2,2´:6´,2´´-terpyridine
µs	microsecond
VR	vibrational relaxation

1 Our choice

Humanity is facing several challenges in the coming decades. Poverty, lack of fresh water supplies, climate change and an ever increasing demand for energy are just a few examples. Energy is essential for all life including human beings all over the world. It is needed for production of food, for heating or cooling of houses, for driving vehicles and for electricity supply. We know that large emissions of greenhouse gases due to combustion of fossil fuels are not sustainable. Furthermore, in the future an increasing number of people will reach the same living standard as in Europe and North America. According to the UNDP report "World energy assessment" from 2000, a reasonable scenario is a doubling of the energy consumption by 2035 relative to 1998, and a tripling by 2050, if the global growth rate of about 2% per year continues. The need for new sustainable energy sources is obvious.[1]

In principle, there are three different potential energy sources that can meet the demands of the energy supply problem, given the amount of energy they must be able to provide, and the technical developments that can be anticipated. Geothermal energy from the interior of the earth can, theoretically, provide us enough energy, but technological breakthroughs are needed to utilize the potential of this energy source. Nuclear power (fission and/or fusion) is another option, but would mean construction of an enormous amount of new reactors to generate the energy needed. Also, the risk of nuclear weapons proliferation and waste problems (for fission) are factors that need to be solved before nuclear power can even be considered the energy source of the future. The third option is to convert solar energy into other forms of energy that are more useful for modern society.[1, 2]

During one hour, more energy is provided to earth in the form of solar radiation than the amount consumed by all human activity on earth in one year. The incoming sunlight has a power of ca 1.7×10^5 TW, and depending on latitude the average incoming power during daytime is in the range 0.3 to 1.0 kW/m^2.[1] The global energy consumption in the year 2001 corresponded to an average power of about 13.5 TW.[2] Thus, theoretically the sun can provide us with all the energy we need, even if the conversion is not very efficient. With this in mind, it would be irresponsible not to explore the enormous potential of solar energy conversion for future needs. And therefore, the sun is our choice.

1.1 Inspiration from nature

Much effort is invested in research aiming at more efficient solar energy conversion processes. One example is solar cells, represented by a variety of different types.[3-5] Another approach is to find inspiration in nature itself. For example, green plants convert solar energy into useful fuels, in the process known as photosynthesis.[6] Although the details of every step of the photosynthetic process are still not known, the main features are fairly well understood.[7]

1.1.1 How nature makes fuel I – Photosynthesis in green plants

Natural photosynthesis in green plants is commonly written as in equation 1.

$$6\ H_2O + 6\ CO_2 + \text{solar energy} \rightarrow C_6H_{12}O_6 + 6\ O_2 \qquad (1)$$

This looks like a simple chemical reaction, but this is a deception. In reality the process involves many different and complex reaction steps. The photosynthetic processes can be divided into light driven and "dark", *i.e.* independent of light, reactions. The photo-driven reactions take place in two membrane bound protein complexes, the reaction centers photosystem I and photosystem II (PS I and PS II, respectively). In PS II, an antenna system consisting of chlorophyll molecules absorbs sunlight and funnels the energy to chlorophylls called P680. Excitation of P680 triggers an electron transfer reaction to a nearby electron acceptor. This process creates the first charge-separated state, from which a series of consecutive electron transfer reaction occurs, and eventually ATP and NADPH are formed. This process, in its most efficient form, can be described by equation 2.[8]

$$2\ H_2O + 4\ ADP + 2\ NADP^+ + 8\ h\nu \rightarrow O_2 + 2\ ATP + 2\ NADPH \qquad (2)$$

Every single electron transfer step is slightly downhill in energy. This slows down the back-electron transfer reaction, which would lead to loss of absorbed energy. The photo-oxidized $P680^+$ is reduced by electrons from water, originating from the oxygen evolving complex (OEC) of PS II. Water oxidation takes place at a metal ion cluster consisting of four manganese ions and one calcium ion, linked together mainly by μ-oxo bridges and amino acids with carboxylic acid side chains. Electron transfer from the OEC to $P680^+$ takes place via a tyrosine residue, and is coupled to proton transfer as well.[7, 9] The whole process is schematically illustrated in Figure 1.

Water oxidation at the Mn-cluster takes place in four steps, where the oxidation power is stored as higher oxidation states of the manganese ions, as the process continues until it finally can oxidize two water molecules, according to equation 3.

$$2\ H_2O \rightarrow O_2 + 4\ H^+ + 4\ e^- \quad (3)$$

If this process could be used to make useful energy carriers such as hydrogen, instead of ATP and NADPH, these can be used as *e.g.* vehicle fuel or to meet other energy demands. Thereby it would be possible to produce fuel directly from sunlight and water.

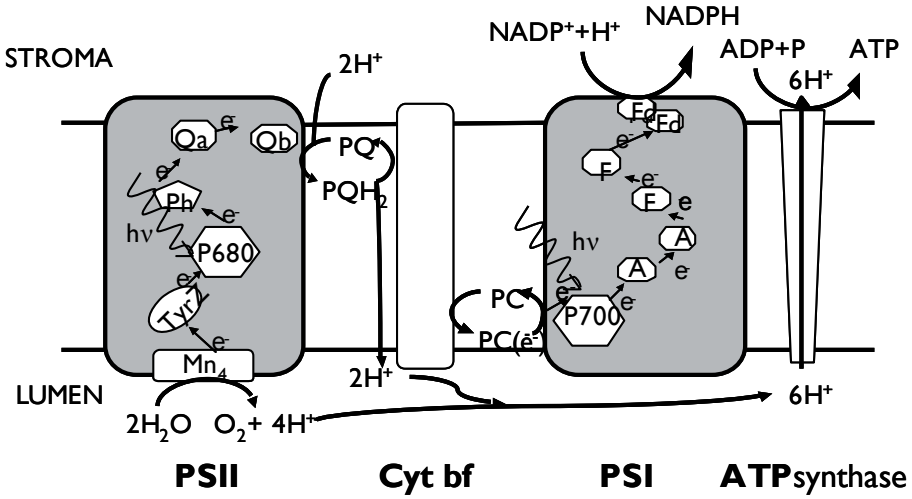

Figure 1. A schematic picture of the main units of photosynthesis, showing the electron flow from water via the membrane bound protein complexes; PS II, Cyt bf and PS I. A proton gradient builds up over the membrane and is used to produce ATP. For a more detailed description any basic biochemistry textbook is useful.

1.1.2 How nature makes fuel II – Hydrogenases as a model

In some green algae, such as *Chlamydomonas reinhardtii,* light-induced reduction of protons can occur.[10] These processes are triggered by photosynthetic reactions where the released electrons are transferred to enzymes called hydrogenases. The hydrogenases can act as catalysts for either the oxidation of dihydrogen (H_2) to protons (H^+), or the reverse reaction, *i.e.,* the reduction of protons into H_2, according to equation 4.

$$2H^+ + 2e^- \rightarrow H_2 \quad (4)$$

The so-called Fe-hydrogenases show higher rates for hydrogen production than for hydrogen consumption. They are interesting as model complexes since they provide another example of how nature makes fuel. If the processes controlling the photo-induced proton reduction can be understood in

detail, it can provide a way to make use of the protons released in the water oxidation step in photosynthesis.[11]

1.2 Mimicking nature – Artificial photosynthesis

With nature as a source of inspiration, many different approaches to achieve conversion and storage of solar energy can be applied[6]. Much effort has been made to find effective light-harvesting devices, based on a donor-photosensitizer-acceptor approach, aimed for photo-induced long-lived charge-separation. Some of the more important work includes a porphyrin-quinone-quinone system reported in 1983,[12] a carotene-porphyrin-quinone complex[13] also in 1983, an amine-porphyrin-quinone system from 1985[14], and in 1987 a phenothiazine-ruthenium-paraquat complex was published.[15]

1.2.1 Artificial photosynthesis

The goal of the artificial photosynthesis work presented in this thesis, performed in the framework of the Swedish consortium for artificial photosynthesis, is a functional, not a structural, mimic of PS II. Identification of key reactions, structures and mechanisms are needed if we should be able to perform artificial water splitting and hydrogen production, induced by sun light.[6, 16-19]

At least three different molecular units are needed to construct an artificial photosynthesis system. This is schematically illustrated in Figure 2. First of all, a photosensitizer (**P**) is needed. The photosensitizer must be able to absorb light and transfer an electron to the electron acceptor (**A**). That is, the photosensitizer should mimic the function of P680. The hole on **P** must be filled by electron transfer from the electron donor (**D**) which mimics the oxygen evolving complex. After this process has been repeated four times, the electron donor should take up four electrons from water, *i.e* oxidize two water molecules, and thereby returning the whole system to its original state, and thereby, the process can start all over again.

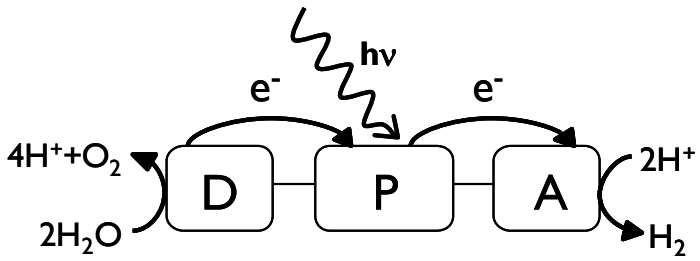

Figure 2. Schematic picture of the three necessary building blocks of an artificial photosynthetic system, where **D** denotes the electron donor capable of oxidizing water, **P** the photosensitizer collecting the sunlight and **A** the electron acceptor capable of reducing protons.

To mimic the donor side of PSII various manganese complexes have been used.[18, 20-22] Attempts using ruthenium have also been made, but with limited success (paper IX). With manganese complexes on the other hand, it has been shown that a photooxidized Ru^{III} can oxidize Mn^{II} in a covalently linked, synthetic complex.[20] Accumulative electron transfer has been observed in a Ru^{II}-$Mn_2^{II,II}$-complex where the Mn-unit could be sequentially oxidized from $Mn_2^{II,II}$ to $Mn_2^{III,IV}$.[22]There are some reports of dinuclear manganese and ruthenium complexes performing catalytic water oxidation by the use of external oxidants, although the exact mechanism is debated.[23-25]

Different electron acceptors have been used to prove that electron transfer reactions from a photosensitizer to an electron acceptor are possible.[26, 27] However, the hydrogen evolving side of artificial photosynthesis has just only recently been explored. Again, a functional mimic of the catalytic site of iron hydrogenases is the goal, and much effort is invested in research areas such as modeling studies as well as mechanistic and functional studies of the enzyme.[28, 29] So far, electrochemical catalytic hydrogen production has been shown[30] but attempts to drive the reaction with photons have not yet succeeded.[31, 32] (paper X).

Light-harvesting is very important for a functional artificial photosynthesis system and therefore the photosensitizer is of prime importance. Nature uses chlorophyll, but this is not a good candidate for an artificial system due to its low stability upon photoexcitation. In principle, aromatic organic molecules can be used, but the short lifetime of their excited states and unfavorable redox properties, together with, typically, high-energy absorptions make them less useful. One exception, however, is the chlorophyll-like porphyrin family, commonly used as photosensitizers in artificial photosynthetic devices as well as for other applications.[33, 34] The third commonly used class of photosensitizers is transition metal complexes. Typical examples are Re^{I}-, Os^{II}- and, most commonly, Ru^{II}-complexes.[35-37]

Although processes like proton–coupled electron transfer[6, 38-41] and accumulative electron transfer[42, 43] are very important for artificial photosynthesis, the photosensitizer is of as great importance. Ru^{II}-complexes, the main theme of this thesis, are not only used as photosensitizers in solar energy conversion, but are also relevant for various applications such as molecular electronics,[44, 45] and light emitting devices[46], molecular sensors and switches[47], molecular machines[48] and also as therapeutic agents[49]. The advantages of Ru^{II}-complexes are high photostability, good absorption properties and fairly long-lived excited states.[37, 50] However, a perfect photosensitizer needs to fulfill several requirements which are seldom all found in the same complex. The goal of the work presented in this thesis was to study and improve the properties of Ru^{II}-based photosensitizers, and more specifically how to tune the excited state properties to make bis-tridentate complexes more suitable for artificial photosynthesis applications. However, the findings in this project may be of interest also for other possible applications for a photosensitizer.

2 Photosensitizer requirements

A good photosensitizer has to fulfill several important general requirements, irrespective of which application it is aimed for. Furthermore, depending on its use, specific prerequisites may apply. Therefore, the properties of the photosensitizers in use are to a large extent compromises between wanted and unwanted properties. This chapter discusses the requirements on photosensitizers aimed for absorption of sunlight to drive further electron transfer reactions, as in artificial photosynthesis.

2.1 Stability

A good photosensitizer must be stable, both in its ground and excited states, as well as in various redox states. In order to function properly, the photosensitizer should also be inert to side reactions, so that it can be used over and over again to promote the desired electron transfer reactions. Obviously it must also be stable towards light-induced decomposition.

2.2 Absorption properties

A strong absorption, *i.e.* a high molar absorption coefficient, in a suitable spectral region is essential for a good photosensitizer. It is important that the photosensitizer can capture photons efficiently and therefore it must absorb in the region where the sun emits radiation. A cartoon-like sketch of the solar radiation intensity variation with wavelength is shown in Figure 3. Around 40% of the sun intensity on earth falls in the range 300-600 nm, which is also the region where most natural pigments absorb. For transition metal complexes based on Ru^{II}, Os^{II} and Re^{I} the desired absorption is normally a metal to ligand charge transfer transition (MLCT transition). In the case of Ru^{II}-complexes this band is normally observed between 400 and 600 nm.[37, 50]

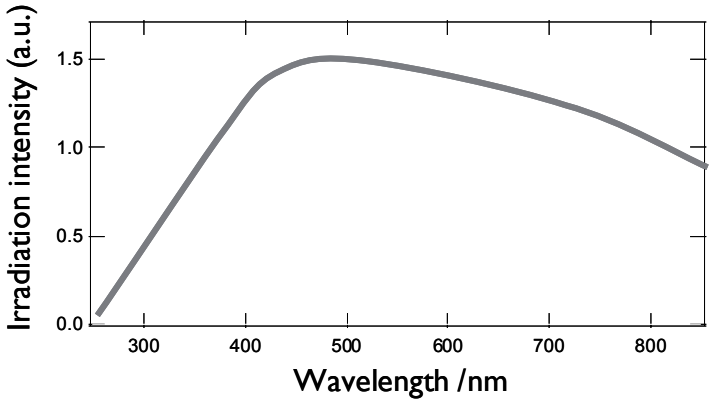

Figure 3. Schematic picture of the sun irradiation intensity distributed over wavelength.[51]

2.3 Redox properties

A fundamental requirement is that the oxidized or reduced photosensitizer, in its ground state, should be a stable species. Furthermore, both the oxidation and the reduction processes must be fully reversible.[37] For the electron transfer processes, the relevant thermodynamic parameters are obtained from the oxidation and reduction potentials of the photosensitizer.

2.4 Geometrical considerations

Ideally, the electron acceptor and donor should be well separated in space in order to reduce unwanted interaction and fast back reactions. Therefore, a linear construction of a **D-P-A** array is preferable. However, a potential problem when covalently attaching electron donor and acceptor moieties to the photosensitizer is the possible formation of different geometrical isomers. Isomer formation reduces the spatial control of donor and acceptor with respect to each other and may lead to complex kinetics and unwanted fast back electron transfer reactions. This problem is illustrated in Figure 4, using Ru^{II}-tris-bipyridine and Ru^{II}-bis-terpyridine as model compounds. Here, the great advantage of tridentate ligands over bidentate ligands is illustrated clearly by a comparison of the model complexes $[Ru^{II}(tpy)_2]^{2+}$ and $[Ru^{II}(bpy)_3]^{2+}$. For bis-tridentate complexes substitution in the 4´-position of the central pyridine ring will automatically lead to a linear, or at least a quasi-linear array, where the electron acceptor and donor will be well sepa-

rated in space. This can be obtained also for the tris-bidentate complexes, as is shown in Figure 4 but other isomers will form as well. Thus, from a geometrical point of view, photosensitizers based on tridentate ligands are the most interesting alternatives.[35, 52]

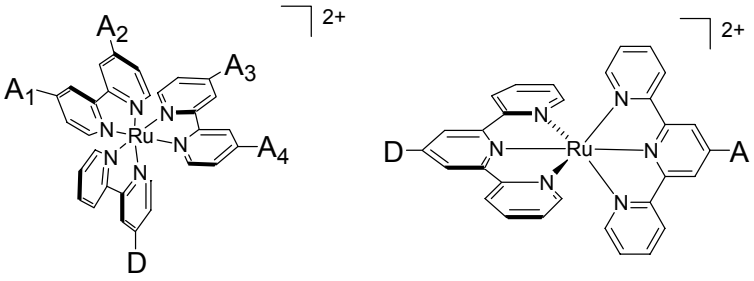

Figure 4. Left: Possible geometrical isomers of $[Ru^{II}(bpy)_3]^{2+}$ upon substitution of electron donor (**D**) and acceptor motifs (**A**). Right: shows that it is possible to obtain rod-like molecular arrays upon substitution on the central pyridines on $[Ru^{II}(tpy)_2]^{2+}$.

2.5 Excited state properties

The key to a functional photosensitizer is its excited state properties, since the desired reactions occur from the excited state. Most important are the excited state lifetime, the excited state energy, and the emission quantum yield. The excited state lifetime has to be long enough to allow for the desired electron transfer reactions to occur before the sensitizer relaxes back to its ground state. Excited state energy is also very important since it sets the limit for the driving force for further electron transfer reactions. Finally, the emission quantum yield, Φ, should ideally be high. A high emission yield provides the possibility of using the emission properties as probe to measure and understand the photophysical behavior. The excited state lifetime and the emission quantum yield are related, but the emission quantum yield is not necessarily proportional to the excited state lifetime. Excited state properties are generally very sensitive to the structure of the complex and can be tuned in several ways, including *e.g.* appropriate choice of ligands and substituents, as will be discussed in chapter 5.[37]

3 Interaction between light and matter – Molecular photophysics

The interaction between light and matter is a fascinating topic and provides the basis for the photosynthetic processes. The fundamental processes of absorption and deexcitation of a molecule must be understood, if prediction and control of photosensitizer properties should be possible. This chapter deals mainly with the photophysical aspect of the excited molecules, *i.e.,* the excitation and the deactivation of the excited state, without any chemical reaction occurring. For a more detailed description see for example references [50] and [53]. Photochemistry requires that a chemical reaction occurs, or at least that a chemical change is induced in the molecule of interest, and different photochemical processes will be discussed briefly.

3.1 Electronically excited states

An optically excited molecule is the result of absorption of electromagnetic radiation, that is, light. Electromagnetic radiation consists of an oscillating electric field and an orthogonal oscillating magnetic field. In electric dipole transitions the molecule interacts with the electric component of the electromagnetic field. Upon absorption of a photon, one electron is transferred from a lower to a higher quantum state of the molecule.

The electronically excited state is obviously energetically unstable, and therefore has to get rid of this extra energy. This can occur via different decay processes, that are either of radiative or nonradiative character. In Figure 5, a Jablonski diagram, *i.e.* a simplified energy level diagram of the possible processes is depicted. Electronic states are characterized by their multiplicity, that is singlet states with paired electron spins and triplet states with unpaired electron spins. An excited triplet state is usually lower in energy than its singlet state counterpart. The size of the system, *e.g.* atoms, small or large molecules as well as the surroundings, *e.g.* gas phase, solution or solid state can significantly affect which transitions that can be probed. The description presented here is valid for large molecules in solution.

Absorption occurs from the ground state, which is often a singlet state, therefore here denoted S_0, to a vibrationally excited level of an electronically excited state, S_n, of the same multiplicity as the ground state. The vibrational

population collapses into the lowest vibrational level of S_n, in a process called vibrational relaxation (VR). The excited state can thereafter be deactivated via different processes of emissive or non-emissive character. Internal conversion (IC) can occur, which corresponds to a radiationless transition to vibronically excited states of the ground state S_0. Another important radiationless deactivation process is the intersystem crossing (ISC), which occurs between excited states of different spin multiplicity, *e.g.* from a singlet to a triplet state, or vice versa. From the lowest excited state of a given multiplicity, that is, S_1 and T_1 state respectively, radiative transitions can occur.

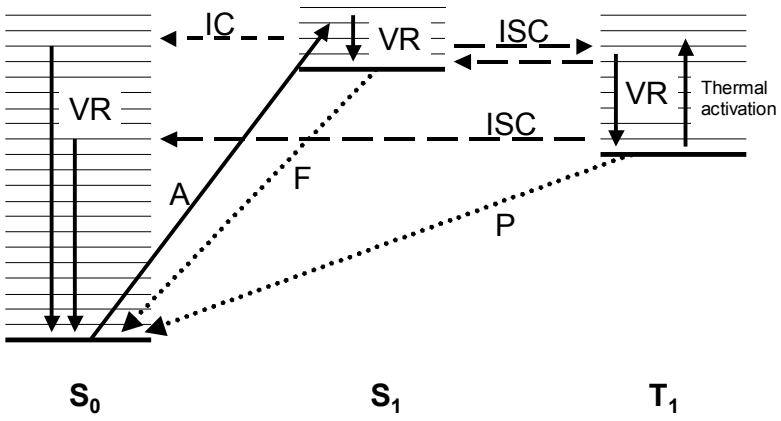

Figure 5. Jablonski diagram showing the possible radiative and nonradiative processes discussed in the text. Note that the S_1 state is shown to the right for clarity reasons, not reflecting a real displacement. A denotes absorption, F fluorescence and P phosphorescence.

3.2 The act of light emission – Radiative transitions

The act of light emission provides a possibility of examining the fate of the excited molecules by probing the emission by different spectroscopic techniques. Fluorescence occurs from an excited state with the same spin multiplicity as the ground state, while phosphorescence originates from an excited state of different spin multiplicity. This makes fluorescence a spin-allowed transition, while phosphorescence is not. However, the phenomenon of spin-orbit coupling makes phosphorescence weakly allowed, and consequently, phosphorescence decay is slower than fluorescence. Both types of emission involve electron motion that is more rapid than nuclear motion. For large molecules in solution the vibrational relaxation is so fast that the lowest excited state is formed before any other process of interest can compete. There-

fore all radiative processes will occur from the lowest excited electronic state of a given multiplicity, *i.e.* S_1 or T_1. This is known as Kasha´s rule, to which there are only a few known exceptions.[54]

The most important features of a radiative transition are the observed emission lifetime of the excited state and the frequency factor for this transition. The observed lifetime should not be confused with the natural lifetime, which is defined as the reciprocal of the radiative rate coefficient (equation 5). Under circumstances where other processes than emission compete with the radiative decay, the measured lifetime is reduced compared to the natural lifetime, and can instead be described by equation 6. Furthermore, the radiative rate constant is an important property of a photosensitizer. It is determined from the emission quantum yield and the observed excited state lifetime, equation 7.

$$\tau_{rad}^{0} = \frac{1}{k_{rad}^{0}} \tag{5}$$

$$\tau_{obs} = \frac{1}{k_{obs}} = \frac{1}{\Sigma k_i} \tag{6}$$

The emission quantum yield, as mentioned above, is another important property. It is denoted Φ, and is defined as the number of photons emitted per unit time and unit volume, divided by the number of quanta (*i.e.* photons) absorbed per unit time and unit volume. In practice, quantum yields are measured versus a reference, and calculated according to equation 8, where n and n_{ref} denotes the refractive index of the sample and the reference solution, respectively. Absorption at the excitation wavelength is denoted by Abs and Abs_{ref} while the emission intensity is given by I and I_{ref}. Thus, the quantum yield is a measure of the efficiency of the conversion of absorbed photons into emitted photons. For molecules obeying Kasha´s rule, the quantum yield is independent of the energy of the initially excited state.

$$k_{rad} = \frac{\Phi_{em}}{\tau_{obs}} \tag{7}$$

$$\Phi_{em} = \frac{n}{n_{ref}} \times \frac{Abs_{ref}}{Abs} \times \frac{I}{I_{ref}} \times \Phi_{ref} \tag{8}$$

3.3 Nonradiative deactivation of excited states

Nonradiative transitions involve the conversion of one molecular quantum state to another without emission of light. The nonradiative deactivation can include removal of excess energy by solvent molecules or collisions with other sample molecules. However, here the focus will be on processes occurring between different quantum states of the same molecule, without the need for external perturbation. Nonradiative transitions can, in contrast to the radiative, be considered horizontal, *i.e.* they occur between different states with the same energy, as shown in the Jablonski diagram.

The rate at which transitions occurs is given by the rate of change of the probability of finding a molecule in this quantum state, as a function of time. This rate depends on the overlap of the wavefunctions of the initial and final states. Fermi and Dirac have derived an expression, valid in the weak coupling limit, that predicts the probability per unit time that the population of one electronic state dissipates into another one. This is known as the Fermi golden rule[55] and can be expressed as in equation 9 below

$$k = \frac{2\pi}{\hbar}\left|V_{MN}\right|^2 \delta\left(E_M - E_N\right) \tag{9}$$

The δ-function guarantees energy conservation during the transition. V_{MN} is the interstate coupling between the initial and the final states M and N. In most cases it is valid to split the coupling element into the electronic coupling and the vibrational overlap parts. Often, it can be assumed that the electronic coupling is independent of the nuclear coordinates.

The sum of all the nonradiative transitions can be described by the nonradiative rate constant, which can be expressed as in equation 10 below

$$k_{nr} = \frac{1 - \Phi_{em}}{\tau_{em}} \tag{10}$$

The energy difference between the ground state and the excited state is of importance for the nonradiative decay from the excited state. It has been shown that the closer in energy the excited state and the ground state are, the faster will the nonradiative decay take place. This is known as the energy gap law and has been demonstrated for several types of molecules[56], and Meyer and coworkers have shown that it is valid also for transition metal complexes[57-60].

3.4 Photochemical processes – Excited state quenching

Competing with the intrinsic deactivation pathways, the excited state can take part in different photochemical reactions. This type of reactions can also be considered as a type of nonradiative transitions, although treated separately here.

In the case of energy transfer (EnT) the excitation energy is transferred to an acceptor molecule, as described by equation 11. The acceptor molecule can be covalently linked to the excited species, or energy transfer can occur via a bimolecular process. Energy transfer can be of Dexter or Förster type, depending on factors such as how close the molecules are and the spectral overlap between the donor and the acceptor.

Dexter type energy transfer[61], also referred to as electron exchange energy transfer, involves the simultaneous transfer of an electron from the excited photosensitizer lowest unoccupied molecular orbital (LUMO) to the LUMO of the acceptor and from the highest occupied molecular orbital (HOMO) of the acceptor to the HOMO of the photosensitizer. Since this is an exchange mechanism, it requires that the molecules are closely associated or that the EnT proceeds via the superexchange mechanism in covalently linked molecules.

Förster type energy transfer[62] is a dipole-dipole interaction and can operate over distances up to 100 Å. The rate depends on the dipole strengths of the transition and the relative orientation of the dipoles and the distance between the photosensitizer and the acceptor. Most important however is, that since the process require resonance, the absorption of the acceptor has to overlap with the emission from the photosensitizer.

Electron transfer (ET) is an interesting photochemical process that converts the excitation energy into chemical energy. It is an important process in PS II but also in many other biological systems and processes. Electron transfer can be either of oxidative or reductive nature, as described by equations 12a and 12b, respectively. As in the case of energy transfer, electron transfer can occur from the photosensitizer either to a covalently linked acceptor or via a bimolecular process in solution.[37]

$$*P^{2+} + Q \rightarrow P^{2+} + *Q \qquad \text{EnT} \qquad (11)$$

$$*P^{2+} + Q \rightarrow P^{3+} + Q^{-} \qquad \text{Oxidative ET} \qquad (12a)$$

$$*P^{2+} + Q \rightarrow P^{+} + Q^{+} \qquad \text{Reductive ET} \qquad (12b)$$

The excited state energy is of importance for electron transfer reactions since an excited molecule is always both a stronger oxidant and a stronger reductant than its ground state counterpart. This is because the excitation energy can be used to drive the photochemical reactions. Electrochemical potentials

are important properties of the photosensitizer and the electron donor and acceptor respectively. The driving force for a ground state reaction can be calculated from equation 13a:

$$\Delta G^0 = e(E_{½}(P^{ox/red}) - E_{½}(A^{ox/red})) + w_p - w_r \quad (13a)$$

In this equation, $E_{½}$ is the reduction potential for the photosensitizer and the acceptor, respectively, w_p and w_r are work terms arising from the coloumbic interaction, and e is the elementary charge. For the corresponding photoinduced one electron transfer reaction, the driving force can be calculated from the Rehm-Weller equation, equation 13b,[63]

$$\Delta G^0 = (E_{½}(P^{ox/red}) - E_{½}(A^{ox/red})) - E^{00} + w \quad (13b)$$

where E_{00} corresponds to the excited state energy of the lowest excited state, and the coloumbic interaction is summarized in w.

4 Photophysical and electrochemical properties of Ru^{II}-polypyridyl complexes

Ru^{II}-polypyridyl complexes are, as mentioned earlier, due to their favorable photophysical properties commonly used as photosensitizers in many different applications. Other transition metals, such as Os^{II} Re^{I} and Ir^{III} can also be used[35, 36], but this chapter will focus on $Ruthenium^{II}$-complexes, their properties and how they can be tuned to work even better. The striking differences between tris-bidentate, *e.g.* $[Ru^{II}(bpy)_3]^{2+}$ and bis-tridentate, *e.g.* $[Ru^{II}(tpy)_2]^{2+}$ complexes will also be discussed.

4.1 The excited state manifold of Ru^{II}-polypyridyls

A schematic picture of the excited state manifold and the related photophysical properties is shown in Figure 6. Although cartoon-like, this picture satisfactorily accounts for the different observations of the excited state decay dynamics and the photochemical reaction pathways, including radiative, nonradiative and activated processes.[35, 37, 50, 64-67].

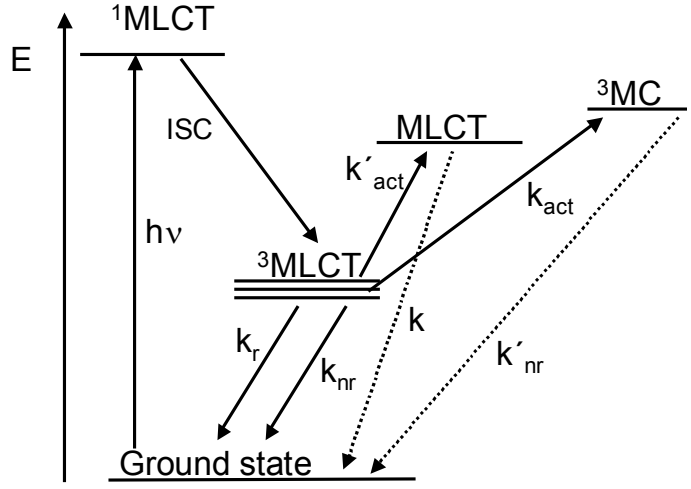

Figure 6. Schematic description of the excited state manifold of Ru^{II}-polypyridyl complexes. The rate constants are denoted k together with a suffix indicating the type of transition.

Upon optical excitation, the lowest excited ^{1}MLCT state will be populated. Due to the heavy atom effect, a fast spin flip will occur and in less than 1 ps the lowest ^{3}MLCT state will be populated, with a quantum yield close to unity.[68, 69] This ^{3}MLCT state is believed to consist of a cluster of three close-lying excited states, with a total energy gap of around 100 cm^{-1}. The splitting into several states is due to low symmetry. The three states have similar but not identical properties. However, at temperatures above 77 K, the three states can be treated as one single ^{3}MLCT state.[65]

In the absence of an external quencher of any kind, the decay from the ^{3}MLCT state mainly occurs via emission to the ground state, via nonradiative decay to the ground state or via thermal activation to higher lying excited states, *i.e.* triplet metal-centered (^{3}MC) states or higher MLCT states. The existence of a fourth MLCT state is indicated from emission polarization measurements, as well as temperature dependent emission studies.[50, 70-73] This higher MLCT state is believed to be more singlet in character and is therefore, more short-lived than the lowest ^{3}MLCT state. It is reported to be between 400 and 1000 cm^{-1} higher in energy than the lowest excited state.

Depending on the energy difference between and ordering of the ^{3}MLCT and ^{3}MC states, the thermal activation can either result in the establishment of equilibrium between the lowest ^{3}MLCT state and a higher state, or irreversible thermal activation leading to decay through the ^{3}MC state. Once in the ^{3}MC state the nonradiative decay is typically very fast, due to large structural distortion with respect to the ground state. This is a prominent deactivation pathway for many excited Ru^{II}-polypyridyl complexes. If the energy gap between the emissive ^{3}MLCT state and the ^{3}MC state is small, this will consequently decrease the observed excited state lifetime significantly. $[Ru^{II}(tpy)_2]^{2+}$ and related bis-tridentate complexes typically have a smaller ^{3}MLCT-^{3}MC energy gap than $[Ru^{II}(bpy)_3]^{2+}$, and thus significantly shorter excited state lifetimes at room temperature. Consequently, the relative energy ordering as well as the energy difference between the different excited states are very important for the photophysical behavior of Ru^{II}-polypyridyl complexes.

Although the description in Figure 6 is generally true for Ru^{II}-polypyridyl complexes, there are exceptions to the rule, since ligand-centered states can become important as well as so called “dark” charge transfer states, as in the well-known Ru^{II}-dppz- complex.[74-77]

4.2 Stability

Stability is, as mentioned in chapter 2, an important property of the photosensitizer. Although the prototype complex $[Ru^{II}(bpy)_3]^{2+}$ is generally considered photostable, significant degradation of the complex occurs during light exposure. Once the ^{3}MC state is formed, cleavage of Ru-N bonds can

occur resulting in a five-coordinate species. This species can either return to the initial R-N6 compound or, when coordinating anions are present, form a hexa-coordinated species with one monodentate bpy-ligand and a coordinated anion. This species can undergo further rearrangement, either reformation of $[Ru^{II}(bpy)_3]^{2+}$ or complete loss of one bpy-ligand. Normally bis-tridentate Ru^{II}-complexes are more resistant to photosubstitution, since each ligand has three coordinating bonds instead of two. This also explains the low stability of Ru-complexes containing monodentate ligands such as lone pyridines.[37]

4.3 Absorption properties

When π-accepting ligands, such as polypyridyl ligands, are coordinated to Ru^{II}, the complex in its ground state may exhibit intense singlet-singlet MLCT transitions in the visible region. This behavior is common for both tris-bidentate and bis-tridentate complexes, although a red-shift of the absorption maximum wavelength is often observed for the bis-tridentate ones. Metal-centered and ligand-centered transitions can also be identified, in the electronic spectrum. The possible transitions are schematically depicted in Figure 7 and the absorption spectrum of $[Ru^{II}(bpy)_3]^{2+}$ together with indications of the possible transitions are shown in Figure 8. The molar absorption coefficients for the ^{1}MLCT transition are dependent of the ability to delocalize the excited electron over the ligand. Thus complexes with higher electron accepting capabilities have higher molar absorption coefficients.[37, 78]

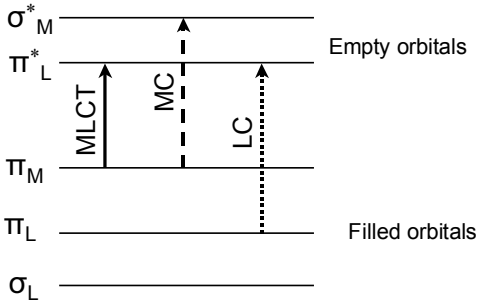

.

Figure 7. Schematic picture of the different absorption processes in Ru^{II}-polypyridyl complexes.

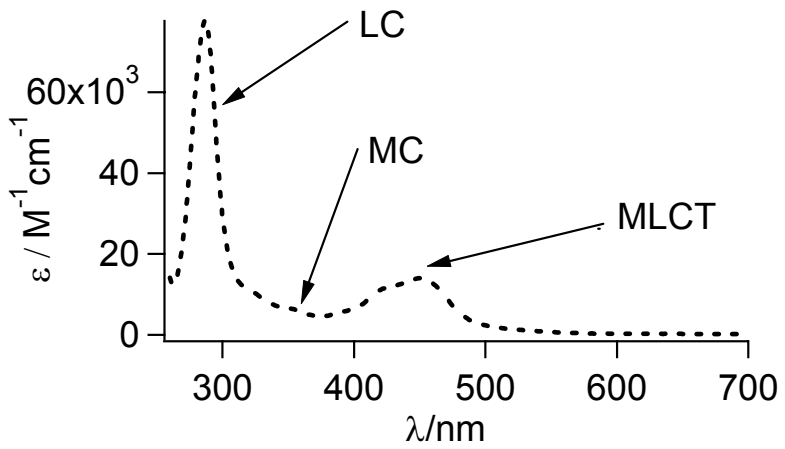

Figure 8. Absorption spectrum for the prototype complex $[Ru^{II}(bpy)_3]^{2+}$, with the transitions described in Figure 7 indicated by arrows.

4.4 Electrochemical properties

Oxidation of a Ru^{II}-polypyridine complex usually involves a metal centered orbital (π_M, t_{2g}), and the formation of a pure Ru^{III}-complex. These are generally inert to ligand substitution, *i.e.* the oxidized species is normally stable, which is an important property for a photosensitizer. For true Ru-polypyridyl complexes, the $Ru^{3+/2+}$ potentials tend to fall in a quite narrow potential range, around 0.9 V measured versus ferrocene ($Fc^{+/0}$) as internal standard. However, if one of the ligands is substituted for another base, this potential can change drastically.[37]

Reduction can in principle involve either a metal centered or a ligand-centered orbital, depending on the relative energy ordering. If the ligands can be easily reduced and/or if the ligand field is sufficiently strong, the reduction takes place on a ligand. Usually, the reduced species is inert, and the process fully reversible. The added electron appears to be localized on a single ligand. In the case of heteroleptic complexes, it is therefore often possible to assign the first reduction to a specific ligand. Often, several different reduction steps can be observed within the accessible potential range. Koopman´s theorem implies that the orbitals involved in the redox processes are the same orbitals as those involved in the MLCT and MC transition respectively.[37] If this is valid, a reversible first reduction implies that the lowest excited state is a MLCT state.

Furthermore, optical energies *i.e.* absorption or emission energies can be correlated to the energy difference between the oxidation and the reduction

potentials. This is based on the assumption that the π* accepting orbital is spatially isolated, and the same for both the reduction process and the charge transfer process, this resulting in a ligand localized excited state, that is a MLCT state.

4.5 Structural influence on the photophysical properties

The geometry of the complex is considered important for the photophysical properties. This can be understood from ligand field theory, which is a combination of crystal field theory and bonding theory. Explained in a simple way, ligand field theory predicts that the orbitals occupied by the d-electrons in a complex must be expected to differ from orbitals of the free ion. Since all Ru^{II}-polypyridyl complexes discussed here have pseudo-octahedral coordination, only the O_h point group, will be discussed. This coordination geometry is of importance for the d-orbitals of the Ru^{II}-ion. In an uncoordinated environment, they are degenerate, but as soon as ligands are introduced, a splitting between the t_{2g} and e_g orbitals will occur, see Figure 9.[79]

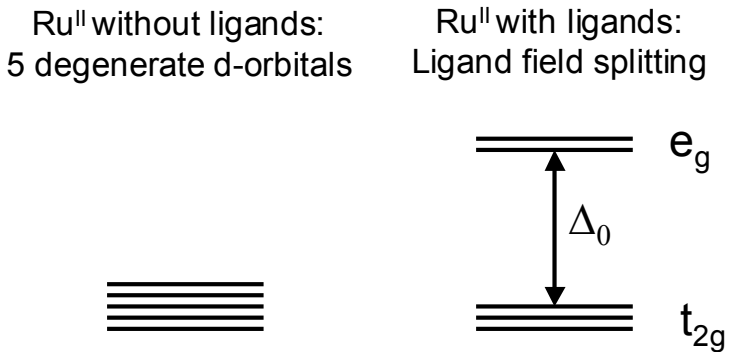

Figure 9. Schematic picture of the splitting between the t_{2g} and the e_g orbitals occuring when ligands are coordinated to the metal. The ligand field strength parameter Δ_0 is also indicated.

The magnitude of this splitting - d-d splitting or ligand field splitting - $\mathbf{\Delta_O}$, depends on 1) the electrostatic field generated by the ligands, 2) the ligand-metal σ-bonding, since the energy of the metal e_g orbitals depends on this factor and 3) the ligand-metal π-bonding since this effects the energy of the metal t_{2g}-orbitals.[80]

The ligand field splitting is obviously a very important parameter since it determines the energy splitting between the metal t_{2g} and e_g orbitals. These are the same orbitals involved in the transition leading to the ^{3}MC excited state. This means that the energy gap between the ^{3}MC and ^{3}MLCT states,

depicted in Figure 6, is dependent on the magnitude of the ligand field splitting. Thus the energy gap can be tuned if it is possible to alter Δ_0 in a controlled manner and this would then be a possible way of tuning the excited state lifetime.

Furthermore, the closer to octahedral the coordination around the metal is, the stronger the ligand field will be. Thus, a stronger ligand field will lead to higher energy of the ^{3}MC state. This implies that the more octahedral a complex is, the longer its excited state lifetime. Consequently tris-bidentate complexes will be better in terms of lifetime, since the bidentate ligands allow for more flexibility than the tridentate ones, and therefore coordination comes closer to a perfect octahedron. Observed properties of numerous bis-tridentate and tris-bidentate complexes supports this prediction.[35, 37]

4.6 Emission properties

The emission properties of Ru^{II}-polypyridyl complexes can provide much information about the properties of the lowest excited state, *i.e.* normally the ^{3}MLCT state, which is important for its function as photosensitizer.

4.6.1 Steady state emission properties

The excited state energy can be estimated from the highest energy peak in the steady state emission spectrum at 77 K.[81-83] Thus, low temperature measurements provide a measure of the energy that can be used as driving force for further electron transfer reactions. The excited state energy can differ significantly between different complexes, from the 2.12 eV reported for $[Ru^{II}(bpy)_3]^{2+}$ to significantly lower energies almost reaching into the IR region. The excited state energy is dependent on the delocalization effect in the ligand as well as the effect of electron donating and accepting substituents on the ligands, and can consequently be tuned by appropriate choice of substituents.

The shape of the emission spectrum at 77 K reveals interesting features. For example, the geometrical distortion of the excited state relative to the ground state can be estimated from the intensity ratio between the second and the first vibronic peaks in the spectrum, thus providing an estimate of the overlap of the vibrational wavefunctions in the ground and excited state.[64]

The quantum yield for emission at 77 K together with excited state lifetime can be used to calculate the radiative and nonradiative rate constants, according to equations 7 and 10, respectively. The radiative rate constant is known to be essentially temperature-independent at temperatures above 77 K. However, the nonradiative rate constant increase with temperature, thus typically causing the observed excited state lifetime to decrease with increas-

ing temperature. Emission quantum yields at 77 K vary between different complexes, but are generally significantly higher than at room temperature.[37]

4.6.2 Time-resolved emission

The observed room temperature excited state lifetime of Ru^{II}-polypyridyl complexes can vary from the picosecond to the microsecond range. At low temperature, most complexes of this type exhibits excited state lifetimes in the microsecond region. The two most important factors that influence the excited state lifetime are the ligand field strength and the excited state energy (by the energy gap law).[37] This means that a more octahedral complex typically will have a longer excited state lifetime than a less octahedral one. Thus, the excited state lifetime is shorter for bis-tridentate complexes than for the tris-bidentate ones, due to the larger strain induced by the more rigid ligand. As described in chapter 2, bis-tridentate complexes have better geometrical properties and thus the very short excited state lifetimes are unfortunate. For example the excited state lifetime at room temperature for $[Ru^{II}(tpy)_2]^{2+}$ is 0.25 ns[35] which cannot compete with the ca 1 μs[37] of $[Ru^{II}(bpy)_3]^{2+}$ for photosensitizer applications. Many different strategies can be used to increase the excited state lifetime of bis-tridentate complexes, and some of them will be described in more detail in chapter 5.

Furthermore, the temperature dependence of the excited state lifetime can provide interesting information about the interaction between the excited states and the different deactivation pathways, both directly to the ground state and via thermal activation to higher lying excited states.

4.7 Localization of the excited state

In a homoleptic complex the excited state can be described either as localized on one of the ligands or delocalized over all of them. The strength of the interligand electronic coupling determines which situation occurs. Resonance Raman studies have shown that the initial excitation is localized on a single ligand.[84] However, it is debated how fast the electron hopping between different ligands really is. Some studies indicate that it happens in a few tens of picoseconds while other reports suggest that the expected high initial anisotropy is lost within a few hundred femtoseconds.[85] For heteroleptic complexes the situation is slightly different. If the ligands have similar LUMO energies the differently localized ^{3}MLCT states will be close in energy, and it may be unclear on which ligand the excited state is actually localized. In spite of similar energies localization on different ligands may yield notably different photophysical properties, as will be discussed in chapter 5. By choice of appropriate substituents on different ligands the lo-

calization of the excited state can be controlled and thus unwanted quenching reactions can be avoided.[21, 86, 87] (discussed in paper IX)

For molecular assemblies in which the Ru^{II}-complex is attached to an electron acceptor or donor via one of the ligands the rates of the subsequent energy and electron transfer processes may change dramatically depending on whether the excited state is localized on the bridging or on a remote ligand. Through bond ET or EnT cannot occur until the excited state is localized on the ligand to which the acceptor is attached.

4.8 Ru^{II}-polypyridyls and their possible use as photosensitizers

As can be seen from the summary above, Ru^{II}-polypyridyls in general fulfill many of the photosensitizer requirements described in chapter 2. However, there are not many complexes that fulfill all the requirements listed in chapter 2.

In summary, Ru^{II}-polypyridyls have many advantages as photosensitizers, but also some disadvantages that have to be addressed before a construction of a functional mimic of PS II can be obtained. The next chapter describes the work of this thesis, aiming at better photosensitizers based on the bis-tridentate type of complexes and how their properties can be tuned.

5 Tuning of the excited state properties of Ru^{II}-polypyridyl complexes

Design of photosensitizers that can be incorporated into linear rod-like molecular arrays needs consideration of all the requirements described in chapter 2. In the present chapter, general strategies to increase the excited state lifetime of the geometrically favorable bis-tridentate Ru^{II}-polypyridyl complexes will be described. Thereafter the work of this thesis will be presented and discussed, focusing on how to make bis-tridentate Ru^{II}-polypyridyl complexes designed for photosensitizing in artificial photosynthesis as well as other applications where longer excited state lifetimes are desirable, including some case studies regarding chelate ring size and localization of the excited state. Finally, the possibility of developing computational methods capable of predicting photophysical properties such as the excited state lifetime will be discussed.

5.1 Strategies to extend the excited state lifetime

The excited state lifetime is a very important property of a photosensitizer. If the photosensitizer should function properly it must be long enough for providing the desired electron an energy transfer, and many different strategies aiming at an extended excited state lifetime have proven successful.[88, 89] The use of electron donating or –withdrawing substituents can increase the excited state lifetime significantly.[88-95] Strong electron withdrawing groups such as SO_2Me attached to the 4´-position of the terpyridine gives room temperature excited state lifetimes of around 30 ns.[93] However electron donating groups will destabilize the metal based HOMO more than they destabilize the ligand-based LUMO and therefore nonradiative decay will be facilitated. Electron withdrawing substituents will instead lower the ^{3}MLCT excited state energy due to a greater stabilization of LUMO as compared to the metal-based HOMO.[89]

Another approach is to use strong σ-donating ligands.[90, 95-98] They will cause a stronger bond to the metal, thus increasing the energy of the metal centered excited state. However this approach is also often associated with a significant lowering of the excited state energy, which limits the chemical reactivity of the excited species. Examples of strong σ-donors are car-

benes,[96] where an excited state lifetime of 820-3100 ns, and emission maximum around 530 nm are reported. The excited state lifetime however shows a very strong and unusual solvent dependence. A peculiar emission rise-time of a few hundred ns was present in their water data but not explained, which suggests that this particular result should be taken with caution. Another example of strong σ-donors are anionic triazoles[91] where the excited state lifetimes are significantly extended and ranges from 24 to 77 ns, while the excited state energies are significantly lowered. Cyclometalated ligands are strong σ-donors which exhibit enhanced luminescence properties but are so low in excited state energy that the energy gap law decreases the excited state lifetime substantially.[97-101]

Another approach that has proven successful is to use extended π-systems to increase the excited state lifetime.[102-108] Excited state lifetimes are significantly prolonged resulting in observed excited state lifetimes between 1 and 43 ns.[35, 109] This effect is due to the fact that attached aromatic groups can conjugate with low-lying π*-levels in the terpyridine ligand, and consequently create an extended π-system, that can delocalize the excess electron density more effective. However, the increased delocalization will also cause a stabilization of the excited state energy, which is observed as well.[83, 105-107, 109]

The last approach to be discussed here is to increase the excited state lifetime by the use of bichromophoric systems, with an intrinsically long-lived organic triplet at a somewhat lower energy than the ^{3}MLCT state, serving as an energy reservoir. If this strategy should result in a longer excited state lifetime the electronic coupling between the different chromophores must be minimized so that the individual electronic properties are maintained. This approach often results in very long excited state lifetimes but bi-exponential decays are frequently observed. The gain in emission lifetime is however exactly counterbalanced by a loss in reactivity because the fractional population of the MLCT state is correspondingly small. Thus the yield of photoreaction from the MLCT state would not increase by this approach, as demonstrated by the fact that the MLCT emission yield is as low as in the reference complexes without organic chromophore. Furthermore, the addition of the extra chromophore will also destroy the possible construction of linear rod-like molecular arrays.[88, 110-119]

5.2 A new design strategy to increase the bite angle in Ru^{II}-bis-tridentate complexes (I-VI)

As seen from the summary above it is not an impossible task to increase the excited state lifetime of Ru^{II}-polypyridyl complexes based on tridentate ligands. However, if all the requirements described in chapter 2 should be

fulfilled and the driving force for further reactions be high enough, a new approach that does not stabilize the ^{3}MLCT state but rather destabilizes the ^{3}MC state has to be developed. A possible solution is provided by ligand field theory. As described in chapter 4, a more octahedral structure will induce a larger splitting between the t_{2g} and e_g orbitals, and consequently the interaction between the electronic states arising from metal-to-ligand and metal-to-metal transitions will be smaller. A larger energy gap would ideally result in a longer excited state lifetimes due to a higher activation barrier for thermally activated decay of the ^{3}MLCT state, see Figure 10. In contrast to the strategies described above, this strategy does not necessarily lead to a stabilization of the excited state energy.

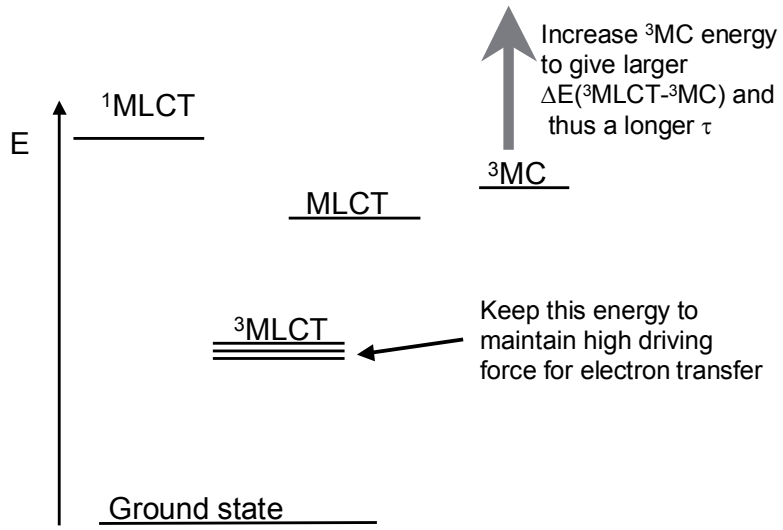

Figure 10. Description of our design strategy to extend the excited state lifetime but still maintain the excited state energy of a bis-tridentate Ru^{II}-polypyridyl complex.

A way to accomplish this situation would be to design new tridentate ligands that allow for larger bite angles than those obtained for Ru^{II}-bis-terpyridine. By extension of the chelate rings from the common five-membered (as in $[Ru^{II}(bpy)_3]^{2+}$ and $[Ru^{II}(tpy)_2]^{2+}$) to six-membered chelate rings this can be possible.

5.2.1 First generation: Increased bite angles by modification of terpyridine ligands (I, II, III)

Taking $[Ru^{II}(tpy)_2]^{2+}$ as a starting point for the design of ligands that allow for larger bite angles, the first attempt was to introduce a methylene link

between two of the pyridines in a normal terpyridine ligand. Furthermore, several complexes with different substituents on the methylene were prepared, to investigate the effect of different substituents, see Figure 11. The idea of using different substituents is that restriction of the motion of the lone ligand pyridyls can be achieved and thus induce further increase of the excited state lifetime. All the complexes were prepared in a heteroleptic version, with one ttpy ligand (ttpy is 4′-tolyl-2,2′:6′,2′′-terpyridine), and some also as the homoleptic analogues.

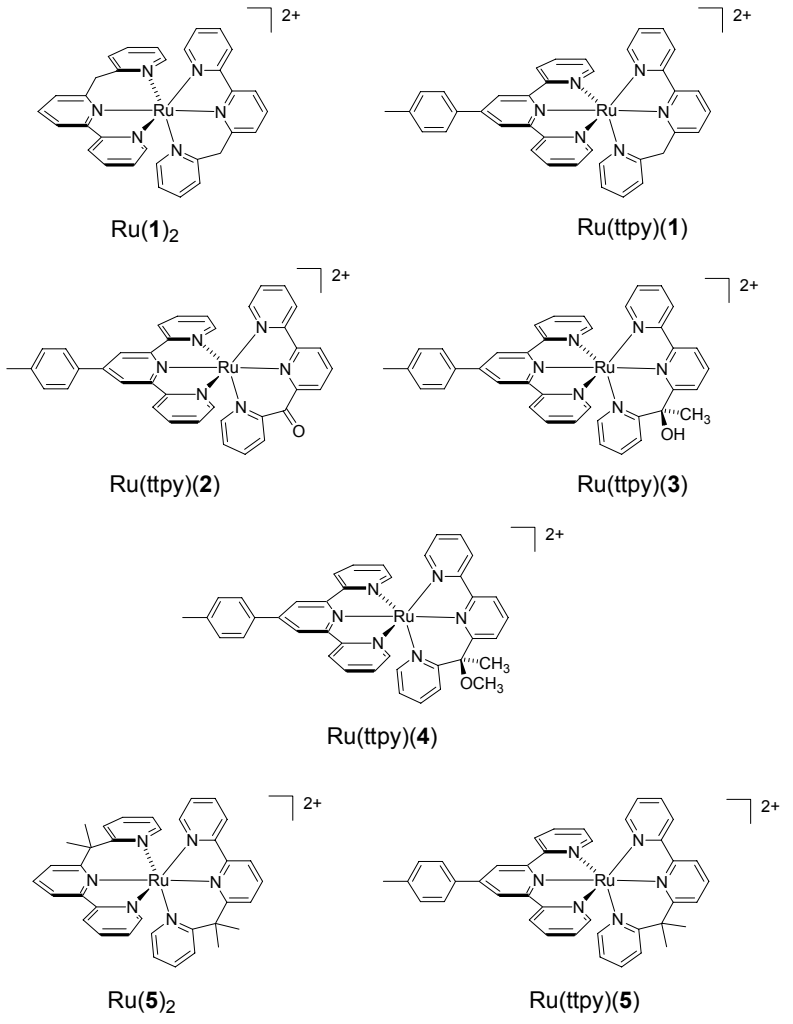

Figure 11. Structures of the complexes investigated in the first generation of photosensitizers.

X-ray structures could only be obtained for $[Ru^{II}(\mathbf{1})_2]^{2+}$, $[Ru^{II}(ttpy)(\mathbf{3})]^{2+}$ and $[Ru^{II}(\mathbf{5})_2]^{2+}$ so additional structural information was obtained by molecular mechanics (MM) calculations as well as density functional theory (DFT) calculations. The crystal structure for $[Ru^{II}(\mathbf{1})_2]^{2+}$ shows bite angles closer to octahedral coordination than that of the parent $[Ru^{II}(tpy)_2]^{2+}$[120], of around 170°. However, the crystal structures also revealed that the additional carbon induces a twist between the bipyridine and terminal pyridine of the ligand, reducing the bite angle. Complexes $[Ru^{II}(ttpy)(\mathbf{3})_2]^{2+}$ and $[Ru^{II}(\mathbf{5})_2]^{2+}$ have ligand bite angles of 165-168°. The MM calculations are in good agreement with the obtained crystal structures for complexes $[Ru^{II}(\mathbf{1})_2]^{2+}$ and $[Ru^{II}(ttpy)(\mathbf{3})]^{2+}$, while DFT is needed to reproduce the geometry of $[Ru^{II}(\mathbf{5})_2]^{2+}$ since MM calculations overestimate the bite angles, suggesting a more octahedral structure than is actually obtained.

When the structural results are compared with the prototype complexes $[Ru^{II}(bpy)_3]^{2+}$ and $[Ru^{II}(tpy)_2]^{2+}$ it is clear that bite angles more close to octahedral coordination can be obtained using this strategy, although the results also indicate that substituents have a pronounced effect on the coordination sphere. If our design idea is correct, prolonged excited state lifetimes should be observed for the complexes (see below).

5.2.2 Second generation: Increased bite angles and more rigid ligands by using phenantroline and quinoline motifs (IV)

The next generation of ligands was based on the same principal design motif, *i.e.* the ligand is built up by mixed five- and six-membered chelate rings. To increase the rigidity of the ligand and hopefully keep the ligand more planar, thus increasing the bite angle even more, another aromatic ring was introduced to create a quinoline. Even more rigidity is infused in the complex by the use of phenatroline instead of bipyridine. In addition to the homoleptic complex an isomeric reference with only five-membered chelates was prepared. The extended π-system in this generation can possibly lead to somewhat lower excited state energies than those obtained for the first generation. The complexes are shown in Figure 12.

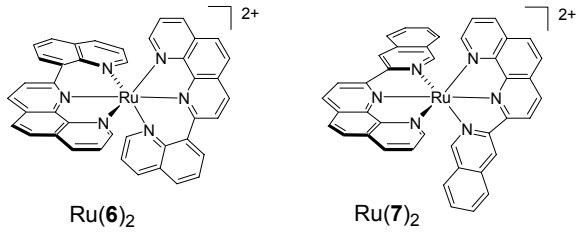

Figure 12. Structures of the complexes investigated in the second generation of photosensitizers.

Crystal structures for $[Ru^{II}(\mathbf{6})_2]^{2+}$ and $[Ru^{II}(\mathbf{7})_2]^{2+}$ could not be obtained, and therefore the geometries were investigated by DFT at the B3LYP/LANL2DZ level of theory. The optimized structures are remarkably different. $[Ru^{II}(\mathbf{6})_2]^{2+}$ has bite angles is close to the desired 180° and the quinoline is twisted 27° out of the plane of the phenantroline. In contrast, the bite angle in $[Ru^{II}(\mathbf{7})_2]^{2+}$ is only 157° according to the calculations, while the angle between the two aromatic systems are 8°. The structural differences predicted by DFT indicates that the photophysical properties of the two complexes are likely to differ significantly, since $[Ru^{II}(\mathbf{6})_2]^{2+}$ has an almost octahedral coordination, while $[Ru^{II}(\mathbf{7})_2]^{2+}$ on the other hand is both less octahedral and can be expected to delocalize the excess electron density better due to its more planar conformation.

5.2.3 Third generation: Increased bite angles and higher symmetry by using quinolines and pyridines (V, VI)

In the third generation of ligands, the rigidity was kept by the use of two quinoline motifs linked via a central pyridine ring, thus the third generation have only six-membered chelate rings. In addition, this ligand design gives the possibility of symmetric attachment of electron acceptors and donors on the central pyridine, that is, along a C_2-axis of the complex (compare with $[Ru^{II}(tpy)_2]^{2+}$ in Figure 4). The homoleptic complex was prepared, and for comparison also the heteroleptic ttpy-complex. To demonstrate the potential of the ligands as building blocks for further construction of rod-like molecular arrays, ester- and amino-functionalized complexes were also prepared. All the complexes are shown in Figure 13.

Compared to the first generation, a lower excited state energy can be expected, due to a larger π-system. On the other hand, they can be expected to have longer emission lifetimes due to more favorable geometrical properties. The crystal structure of complex $[Ru^{II}(\mathbf{8})_2]^{2+}$ and the DFT optimized structure are in good agreement, with ligand bite angles of 179.6° obtained by DFT and 177.6° from the crystal structure, indeed suggesting an almost octahedral complex. A twisted ligand structure is evident, both from calculations and X-ray crystal structure, suggesting dihedral angles of approximately 35° and 39° between the quinolines and the central pyridine.

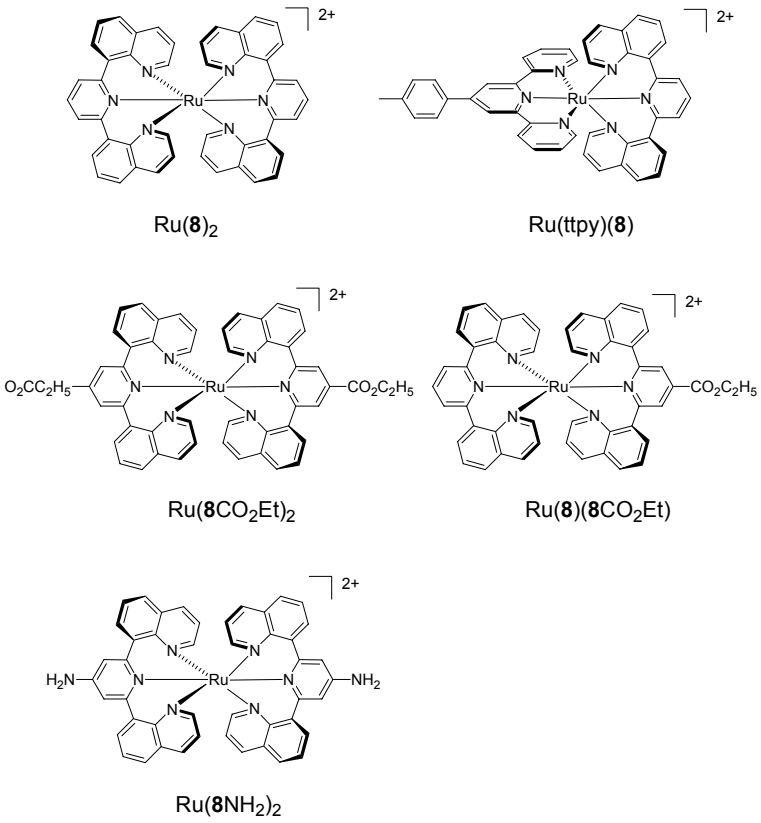

Figure 13. Structures of the complexes investigated in the third generation of photosensitizers.

5.3 Structural influence on electronic absorption spectra and electrochemical properties (I-VI)

5.3.1 Absorption properties

Absorption properties of all the investigated complexes are summarized in Table 1, and typical spectra for every generation are shown in Figure 14. All complexes exhibit the expected ^{1}MLCT-band in the 400-600 nm region. [35, 37] The absorption maxima fall in the range from 474 to 540 nm, with all the modified terpyridine complexes in the blue part, ranging from 474 to 486 nm. The molar absorption coefficients at the ^{1}MLCT maximum wavelength

varies between 0.8×10^4 and 1.7×10^4 $M^{-1}cm^{-1}$. This is in the same range as the parent complexes $[Ru^{II}(bpy)_3]^{2+}$ and $[Ru^{II}(tpy)_2]^{2+}$.[35, 37] For the first generation of complexes all the ttpy-containing compounds exhibit a larger molar absorption coefficient, which is probably due to better delocalization over the larger π-system of the ligand resulting in a larger transition dipole moment. The functionalized complexes based on the bis-quinoline-pyridine system all display structured ^{1}MLCT bands with shoulders in the red part of the band. In the UV-region the spectra are dominated by ligand-centered π→π* transitions.[37, 121]

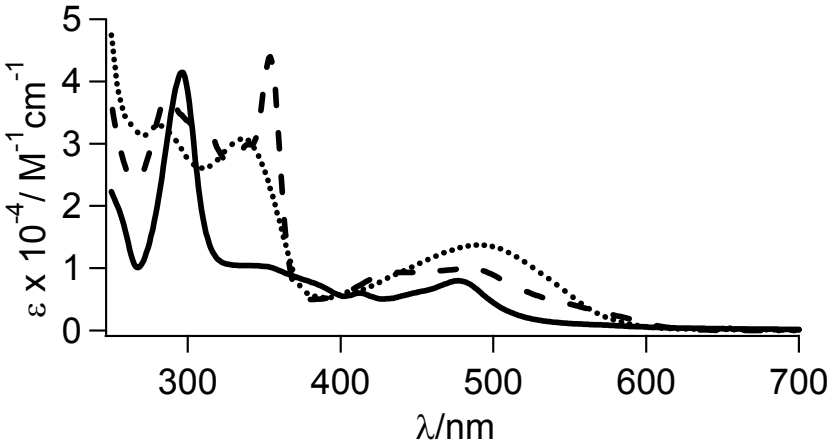

Figure 14. Absorption spectra for $[Ru^{II}(\mathbf{1})_2]^{2+}$ (solid line), $[Ru^{II}(\mathbf{6})_2]^{2+}$ (dashed line) and $[Ru^{II}(\mathbf{8})_2]^{2+}$ (dotted line) in acetonitrile.

Of particular interest is the difference in the electronic absorption spectra between the two complexes in the second generation, since they consist of exactly the same structural motifs, but still differ significantly in their absorption maxima both for the metal-to ligand and the ligand-centered transitions, indicating a clear electronic difference. The absorption intensity are higher for $[Ru^{II}(\mathbf{7})_2]^{2+}$, possibly indicating a better delocalization of the excited state.

Table 1. Electronic absorption wavelength maxima in the visible region and the first electrochemical oxidation and reduction potentials, reported versus $Fc^{+/0}$.

Complex	λ_{max} /nm ($\varepsilon \times 10^{-4}$ /$M^{-1}cm^{-1}$)	$E_{½}$ /V	
		$L^{0/-}$	$Ru^{III/II}$
$[Ru^{II}(ttpy)(\mathbf{1})]^{2+}$	486 (1.5)	-1.61	0.82
$[Ru^{II}(\mathbf{1})_2]^{2+}$	477 (0.82)	-1.67	0.78
$[Ru^{II}(ttpy)(\mathbf{2})]^{2+}$	474 (0.87)	-1.13	0.95
$[Ru^{II}(ttpy)(\mathbf{3})]^{2+}$	482 (1.5)	-1.60	0.79
$[Ru^{II}(ttpy)(\mathbf{4})]^{2+}$	482 (1.7)	-1.60	0.81
$[Ru^{II}(ttpy)(\mathbf{5})]^{2+}$	485 (1.5)	-1.58	0.82
$[Ru^{II}(\mathbf{5})_2]^{2+}$	472 (0.74)	-1.64	0.84
$[Ru^{II}(\mathbf{6})_2]^{2+}$	485 (1.0)	-1.49	0.78
$[Ru^{II}(\mathbf{7})_2]^{2+}$	540 (1.3)	-1.24	0.91
$[Ru^{II}(ttpy)(\mathbf{8})]^{2+}$	457 (1.5)	-1.59	0.78
$[Ru^{II}(\mathbf{8})_2]^{2+}$	491 (1.4)	-1.73	0.71
$[Ru^{II}(\mathbf{8})(\mathbf{8}CO_2Et)]^{2+}$	491 (-)	-1.58	0.77
$[Ru^{II}(\mathbf{8}CO_2Et)_2]^{2+}$	486 (-)	-1.52	0.82
$[Ru^{II}(\mathbf{8}NH_2)_2]^{2+}$	476 (-)	-1.86	0.34

5.3.2 Electrochemical properties

The electrochemical properties of the complexes were investigated by cyclic voltammetry in acetonitrile solutions. All complexes show a metal-based oxidation in the potential range from 0.71 V to 0.95 V (versus the ferrocene/ferrocenium redox couple) and the first reductions occur between –1.13 V and –1.72 V, with most complexes in the range from –1.60 to –1.70 V. A better π-accepting ability can be expected of the ligands in complex $[Ru^{II}(ttpy)(\mathbf{2})]^{2+}$ and $[Ru^{II}(\mathbf{7})_2]^{2+}$ (as indicated also by calculations and electronic absorption data) explaining the observed reduction potentials of range.

The energy gap between the first oxidation and the first reduction is a measure of the energy gap between the HOMO (metal t_{2g}-orbitals) and the LUMO (ligand π-orbitals), and if the redox orbitals are the same as the spectroscopic orbitals a linear correlation between the ^{1}MLCT absorption energy and the energy gap between the HOMO and LUMO, that is $\Delta E_{½}=E_{ox}-E_{red}$ can be expected.[50]

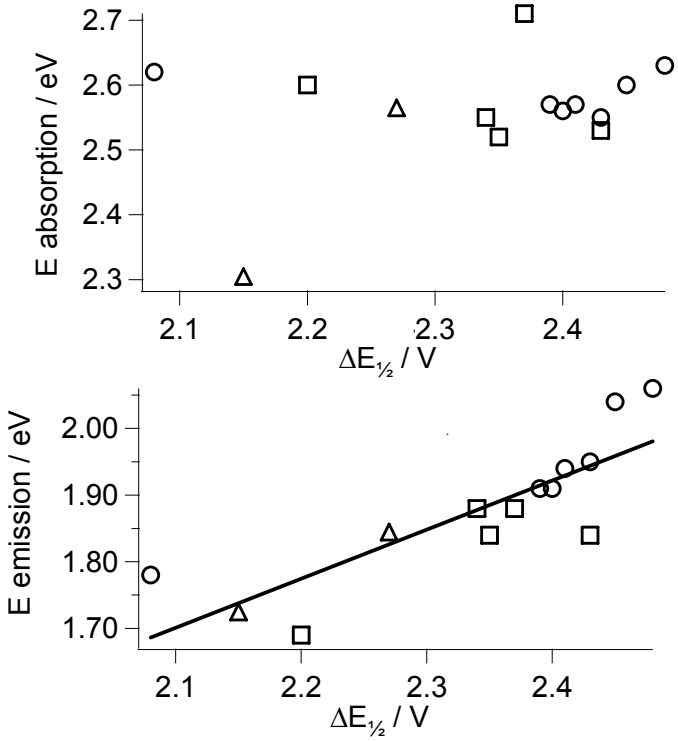

*Figure 15.*Upper: Correlation between absorption energy and electrochemical potentials. Lower: Correlation between emission energy and electrochemical potential. The straight line is the result of a linear fit to all data points, giving a slope of 0.74. Circles: first generation, triangles: second generation, squares: third generation.

Figure 15 shows this correlation for all the complexes. Obviously, the visible absorption maximum is composed of overlapping transitions of MLCT character, and the correlation is poor for this series of complexes. Instead, the correlation of emission energy and $\Delta E_{½}$ is better as emission occurs from the lowest MLCT state manifold, although the data are somewhat scattered. (Figure 15.) A linear fit f the emission data gives a slope of 0.74, which is slightly lower than the expected unity, which however is seldom observed.[37]

5.4 Structural influence on emission properties (I-VI)

5.4.1 First generation: Maintained excited state energy and a 50-fold increase of the excited state lifetime (I-III)

Photophysical parameters for the first generation are summarized in Table 2. The first generation of complexes are all good emitters at low temperature (77 K) and all except complex $[Ru^{II}(ttpy)(\mathbf{2})]^{2+}$ have their maximum emission in the spectral range from 600 and 650 nm, Figure 16. The maximum emission wavelength in a frozen solvent can be taken as a measure of the excited state energy.[81-83] This result is important since it clearly shows that the excited state energy is not significantly lowered by this strategy. The much lower excited state energy of $[Ru^{II}(ttpy)(\mathbf{2})]^{2+}$ can be understood by the better π-accepting ability of the carbonyl functionality in the ligand. The emission quantum yields at low temperature vary between 0.1 and 0.3, which is in the same range as for $[Ru^{II}(bpy)_3]^{2+}$ but significantly lower than $[Ru^{II}(tpy)_2]^{2+}$.[122-124]

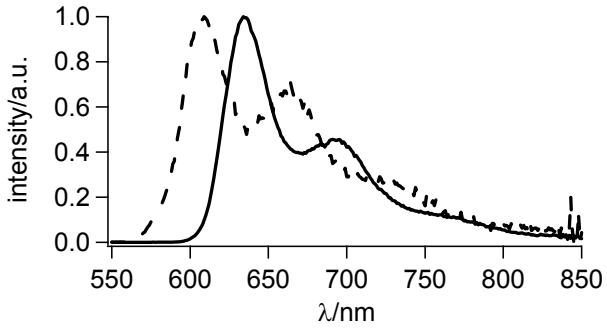

Figure 16. Normalized and detector sensitivity corrected steady state emission spectra for $[Ru^{II}(ttpy)(\mathbf{1})]^{2+}$ (solid line) and $[Ru^{II}(\mathbf{1})_2]^{2+}$ (dashed line).

Most complexes exhibit a more or less well-resolved vibronic structure resulting from the involvement of medium-frequency stretching modes of the polypyridine ligands. The spectral distortion can be judged from the intensity ratio of the second over the first vibronic peak in the emission spectra at 77 K, and is a measure of the difference in the equilibrium nuclear geometry between the ground and excited state. (Meyer, Pure and applied chemistry) Typically, the difference is smaller for a ^{3}MLCT state localized on a terpyridine than on a bipyridine ligand, because the excess electron density is delocalized over a larger ligand leading to a smaller geometrical distortion and consequently a lower relative intensity of the second vibronic peak. Thus, several of the heteroleptic complexes in which the lowest excited state is localized on the ttpy ligand shows a smaller spectral distortion than the homoleptic complexes. The spectral distortion for $[Ru^{II}(\mathbf{1})_2]^{2+}$ is much smaller

than for $[Ru^{II}(bpy)_3]^{2+}$ and instead closer to that for $[Ru^{II}(tpy)_2]^{2+}$. This indicates that the ^{3}MLCT excited state is somewhat delocalized over the entire bipyridyl-pyridyl ligand. The same is true for $[Ru^{II}(\mathbf{5})_2]^{2+}$.

At room temperature all complexes in the first generation are weak emitters with quantum yields in the range from 10^{-4} to 10^{-5}, although it should be noted that complex $[Ru^{II}(\mathbf{1})_2]^{2+}$ shows a remarkable increase in emission quantum yield compared to the parent $[Ru^{II}(tpy)_2]^{2+}$.

The excited state lifetimes at 77 K are all in the range from 2-10 μs, which is in the normal range for most Ru^{II}-polypyridyl complexes. However, the room temperature data are more interesting. The complexes based on ligand **1**, both show increased excited state lifetimes, the heteroleptic complexes of 1.4 ns and the homoleptic 15 ns, which is a 50-fold increase, compared to the parent $[Ru^{II}(tpy)_2]^{2+}$. This is a clear indication that our design strategy works.

However, the other complexes in the first generation are not as good as the two first ones. This can be understood from the structural differences between the complexes. MM calculations, supported by NMR data, suggest that the ligands are not planar when coordinated to ruthenium, and also that there is a considerable amount of interaction between the substituents and the hydrogens of the other ligand, which contributes to a weakening of the ligand field, and consequently a shortening of the excited state lifetime. However, these effects should not give a significant contribution for the complexes in the second generation.

Table 2. Steady state and time-resolved emission results at 298 K and 80 K for the first generation of photosensitizers.

Complex	298 K			80 K		
	λ_{max}/nm	τ/ns	Φ	λ_{max}/nm	τ/μs	Φ
$[Ru^{II}(ttpy)(\mathbf{1})]^{2+}$	655	1.4	2×10^{-4}	637	8.1	0.21
$[Ru^{II}(\mathbf{1})_2]^{2+}$	655	15.0	1×10^{-3}	609	3.7	0.21
$[Ru^{II}(ttpy)(\mathbf{2})]^{2+}$	-	-	-	696	1.9/5.8[a]	0.11
$[Ru^{II}(ttpy)(\mathbf{3})]^{2+}$	655	0.14	4×10^{-5}	650	7.4	0.30
$[Ru^{II}(ttpy)(\mathbf{4})]^{2+}$	650	0.47	6×10^{-5}	639	9.2	0.31
$[Ru^{II}(ttpy)(\mathbf{5})]^{2+}$	-	0.1	$<2\times10^{-5}$	650	5.6	0.44
$[Ru^{II}(\mathbf{5})_2]^{2+}$	650	0.3	1×10^{-4}	603	3.5	0.52

[a] 75% and 25% of the emission intensity respectively

5.4.2 Second generation: An excited state lifetime similar to that for $[Ru(bpy)_3]^{2+}$ (IV)

The emission spectra of the second generation of complexes are more red-shifted than the first generation, 672 nm and 721 respectively for $[Ru^{II}(\mathbf{6})_2]^{2+}$ and $[Ru^{II}(\mathbf{7})_2]^{2+}$ at 77 K. Steady state emission spectra at 80 K are shown in

Figure 17. The significantly lower excited state energy of $[Ru^{II}(\mathbf{7})_2]^{2+}$ compared to $[Ru^{II}(\mathbf{6})_2]^{2+}$ can possibly be explained by a larger delocalization, because of a more planar geometry indicated by DFT results. The emission quantum yields at low temperature are significantly lower than those of both $[Ru^{II}(bpy)_3]^{2+}$ and $[Ru^{II}(tpy)_2]^{2+}$, although even lower quantum yields have been reported for other Ru-polypyridyl complexes. Room temperature steady state emission shows a very redshifted emission of $[Ru^{II}(\mathbf{7})_2]^{2+}$ while $[Ru^{II}(\mathbf{6})_2]^{2+}$ emits around 710 nm. However, more interesting is that the emission quantum yields are around $2\text{-}5\times10^{-3}$ at room temperature. This is both a substantial increase compared to many other bis-tridentate Ru^{II}-complexes, but even more striking is the fact the difference between 80 K and ambient temperatures is much smaller than normally observed. This indicates significantly different photophysical properties for the second generation of complexes. The results are summarized in Table 3.

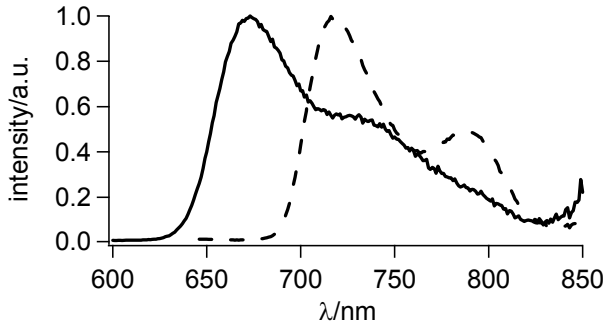

Figure 17. Normalized and detector sensitivity corrected steady state emission spectra for $[Ru^{II}(\mathbf{6})_2]^{2+}$ (solid line) and $[Ru^{II}(\mathbf{7})_2]^{2+}$ (dashed line).

Table 3. Steady state and time-resolved emission results at 298 K and 80 K for the second generation of photosensitizers.

Complex	298 K			80 K		
	λ_{max}/nm	τ/ns	Φ	λ_{max}/nm	τ/μs	Φ
$[Ru^{II}(\mathbf{6})_2]^{2+}$	712	810	5×10^{-3}	672	4.1	0.05
$[Ru^{II}(\mathbf{7})_2]^{2+}$	762	180	2×10^{-3}	721	1.2	0.05

An analysis of the low temperature emission spectral shape can provide information about factors that govern also the nonradiative deactivation of the excited state. This includes vibrational modes that are coupled to the transitions and structural differences between the ground and excited state structure. Following the approach of Meyer and co-workers the low temperature emission spectra were fitted to a series of gaussians according to equation 14.

$$I(E)=\sum_{n_M}\sum_{n_L}\left(\frac{E_{00}-n_M\bar{\nu}_M-n_L\bar{\nu}_L}{E_{00}}\right)^4\left(\frac{S_M^{n_M}}{n_M!}\right)\left(\frac{S_L^{n_L}}{n_L!}\right)\times$$
$$\times\left\{\exp\left(-4\lg 2\left(\frac{E-E_{00}+n_M\bar{\nu}_M+n_L\bar{\nu}_L}{\bar{\nu}_{½}}\right)^2\right)\right\} \quad (14)$$

In this expression, E_{00} is the wave number of the zero-zero electronic transition, ν_M and ν_L are the wave numbers of the vibrational transitions, n_M and n_L are the vibrational quantum numbers, $\nu_{½}$ is the full width half maximum (FWHM) of the gaussians and S_M and S_L are the Huang-Rhys factors, quantifying the nuclear distortion between the ground and excited states as described in equation 15

$$S_i=\frac{\lambda_i}{\hbar\omega_i} \quad (15)$$

where λ_i is the reorganization energy and $\hbar\omega_i$ is the vibrational quantum for the relevant vibrational coordinate. It is usually assumed that one medium and one low frequency vibrational mode is enough to reproduce the experimentally obtained data. The results from the fitting procedure are summarized in Table 4.

Table 4. Spectral fit parameters from 80 K steady state emission measurements. The medium and low frequency modes were locked to 1350 and 400 cm^{-1} respectively. [58, 82, 125]

Complex	E_{00} / cm^{-1}	ν_M / cm^{-1}	S_M	ν_L / cm^{-1}	S_L	$\nu_{½}$ /cm^{-1}
$[Ru^{II}(\mathbf{6})_2]^{2+}$	15060	1350	0.68	400	1.02	770
$[Ru^{II}(\mathbf{7})_2]^{2+}$	13860	1350	0.57	400	0.35	720

While the Huang-Rhys factor for $[Ru^{II}(bpy)_3]^{2+}$ is around 0.95 it is only ~0.5 for $[Ru^{II}(ttpy)_2]^{2+}$ clearly indicating that $[Ru^{II}(\mathbf{6})_2]^{2+}$ and $[Ru^{II}(\mathbf{7})_2]^{2+}$ have a larger degree of delocalization of the excited state than in tris-bidentate complex.[126]

At low temperature $[Ru^{II}(\mathbf{6})_2]^{2+}$ has an excited state lifetime of 4.1 μs, once again in the normal range for Ru^{II}-complexes. However, $[Ru^{II}(\mathbf{7})_2]^{2+}$ is not more long-lived than 1.2 μs, but since its emission is very red-shifted, the energy gap law can explain this behavior. At room temperature the excited state of $[Ru^{II}(\mathbf{7})_2]^{2+}$ lives for 180 ns indicating that although the nonradiative decay directly to the ground state may be substantial, the excited state lifetime is very long for a Ru^{II}-bis-tridentate complex. $[Ru^{II}(\mathbf{6})_2]^{2+}$, which ideally should be better as suggested both by a higher quantum yield at room

temperature and by a higher excited state energy, as well as a more octahedral coordination displays an excited state lifetime at 298 K, actually approaching that of $[Ru^{II}(bpy)_3]^{2+}$, with 810 ns for $[Ru^{II}(\mathbf{6})_2]^{2+}$ compared to the around 1 μs (depending on solvent) for $[Ru^{II}(bpy)_3]^{2+}$. So far, this is the longest room temperature excited state lifetime for a Ru^{II}-complex with tridentate ligands. As other bis-tridentate complexes with similar MLCT energies do not reach excited state lifetimes of several hundred nanoseconds the result cannot be explained simply by a lowering of the MLCT state energy. Instead the results indicate that the MC states are raised in energy thanks to the more octahedral structure of complex $[Ru^{II}(\mathbf{6})_2]^{2+}$.

Since an excited state lifetime of 810 ns is very long for a bis-tridentate Ru^{II}-complex, transient absorption measurements were carried out to prove that the emissive state is really a ^{3}MLCT state. The whole spectral region investigated showed a uniform decay rate constant, equal to the emission decay rate, indicating that the lowest ^{3}MLCT state is the emissive state.

5.4.3 Third generation: Microsecond ^{3}MLCT excited state lifetimes (V, VI)

For the third generation the emission maximum wavelengths at 77 K vary between 660 and 675 nm (Figure 18) except for $[Ru^{II}(\mathbf{8NH_2})_2]^{2+}$ which displays its maximum emission at 735 nm. The emission quantum yields at 80 K are very different for the complexes $[Ru^{II}(\mathbf{8})_2]^{2+}$ and $[Ru^{II}(\mathbf{8})(ttpy)]^{2+}$, the former being similar to the complexes in the second generation while the latter is very similar to $[Ru^{II}(tpy)_2]^{2+}$. Room temperature quantum yields are significantly higher than expected, and of the same order of magnitude as those reported for $[Ru^{II}(bpy)_3]^{2+}$, $[Ru^{II}(\mathbf{8})_2]^{2+}$, $[Ru^{II}(\mathbf{8})(\mathbf{8CO_2Et})]^{2+}$ and $[Ru^{II}(\mathbf{8CO_2Et})_2]^{2+}$, while $[Ru^{II}(\mathbf{8})(ttpy)]^{2+}$ is almost non-emissive, see Table 5. Finally, $[Ru^{II}(\mathbf{8NH_2})_2]^{2+}$ has a very red-shifted emission at room temperature and therefore the quantum yield is not well determined.

The low temperature emission spectra were also fitted to equation 14 and the results are summarized in Table 6.

Table 5. Steady state and time-resolved emission results at 298 K and 80 K for the third generation of photosensitizers.

Complex	298 K			80 K		
	λ_{max}/nm	τ/μs	Φ	λ_{max}/nm	τ/μs	Φ
$[Ru^{II}(ttpy)(\mathbf{8})]^{2+}$	685	7.4×10^{-3}	$<5\times10^{-4}$	660	6.0	0.41
$[Ru^{II}(\mathbf{8})_2]^{2+}$	700	3.0	0.02	673	8.5	0.06
$[Ru^{II}(\mathbf{8})(\mathbf{8}CO_2Et)]^{2+}$	706	4.3	0.04	675	10.7	-
$[Ru^{II}(\mathbf{8}CO_2Et)_2]^{2+}$	693	5.5	0.07	661	11.2	-
$[Ru^{II}(\mathbf{8}NH_2)_2]^{2+}$	~780	0.45	$\sim4\times10^{-4}$	735	2.7	-

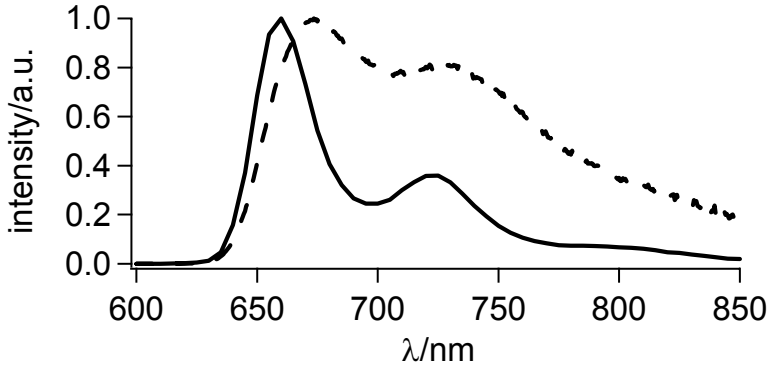

Figure 18. Normalized and detector sensitivity corrected steady state emission spectra for $[Ru^{II}(ttpy)(\mathbf{8})]^{2+}$ (solid line) and $[Ru^{II}(\mathbf{8})_2]^{2+}$ (dashed line).

Table 6. Spectral fit parameters from 80 K steady state emission measurements. The medium and low frequency modes were locked to 1350 and 400 cm^{-1}, respectively. [58, 82, 125]

Complex	E_{00} / cm^{-1}	ν_M / cm^{-1}	S_M	ν_L / cm^{-1}	S_L	$\nu_{½}$ /cm^{-1}
$[Ru^{II}(ttpy)(\mathbf{8})]^{2+}$	15230	1350	0.55	400	0.54	610
$[Ru^{II}(\mathbf{8})_2]^{2+}$	15230	1350	0.96	400	1.7	800
$[Ru^{II}(\mathbf{8})(\mathbf{8}CO_2Et)]^{2+}$	15170	1350	0.62	400	1.42	520
$[Ru^{II}(\mathbf{8}CO_2Et)_2]^{2+}$	15290	1350	0.70	400	1.14	500
$[Ru^{II}(\mathbf{8}NH_2)_2]^{2+}$	13890	1350	0.90	400	1.2	980

The spectral distortion as judged from the S_M value differs significantly between the complexes, with $[Ru^{II}(ttpy)(\mathbf{8})]^{2+}$ being very similar to $[Ru^{II}(ttpy)_2]^{2+}$, indicating that the excited state is localized on the ttpy-ligand. $[Ru^{II}(\mathbf{8})_2]^{2+}$ and $[Ru^{II}(\mathbf{8NH_2})_2]^{2+}$ are more similar to $[Ru^{II}(bpy)_3]^{2+}$ with the ester functionalized complexes falling in between, indicating that ability to delocalize the excess electron density is somewhat different between the complexes.

Time-resolved low temperature measurements show excited state lifetimes between 2.7 and 11.2 μs for the complexes, where the amino functionalized complex with the lowest ^{3}MLCT energy also has the shortest excited state lifetime and the two ester-functionalized compounds have the longest lifetimes.

At ambient temperatures, the excited state of the complexes are ranging from 8 ns for $[Ru^{II}(ttpy)(\mathbf{8})]^{2+}$ once again the exception to the rule, via 450 ns for the low energy $[Ru^{II}(\mathbf{8NH_2})_2]^{2+}$, via 3.0 μs for the $[Ru^{II}(\mathbf{8})_2]^{2+}$, 4.3 μs for the heteroleptic ester complex and 5.5 μs for the homoleptic ester complex. This is the longest excited state lifetimes reported not only for bis-tridentate Ru^{II}-complexes but for any ^{3}MLCT state of a Ru^{II}-polypyridine complex.

There are reports of bichromophoric systems with very long emission lifetimes as well, but that class of compounds is not comparable because the ^{3}MLCT lifetime is not changed, only its fractional population, leading to a longer observed emission lifetime, as discussed in chapter 5.1.[114]

However, the very long excited state lifetimes are actually long enough that ligand-centered rather than ^{3}MLCT-based emission is possible. To prove that the ^{3}MLCT is the emissive state, transient absorption measurements of $[Ru^{II}(\mathbf{8})_2]^{2+}$ were carried out, showing a uniform decay over the spectral range from 350 to 750 nm with the same time constant as the time resolved emission. The resulting transient spectrum is shown in Figure 19. This shows the typical features of excited Ru^{II}-polypyridine complexes with an absorption attributable to the reduced ligand ($\mathbf{8}^{\bullet-}$) around 390 nm, a ground state bleach and an absorption above 580 nm due to LMCT and excited LC transitions.[68, 127]

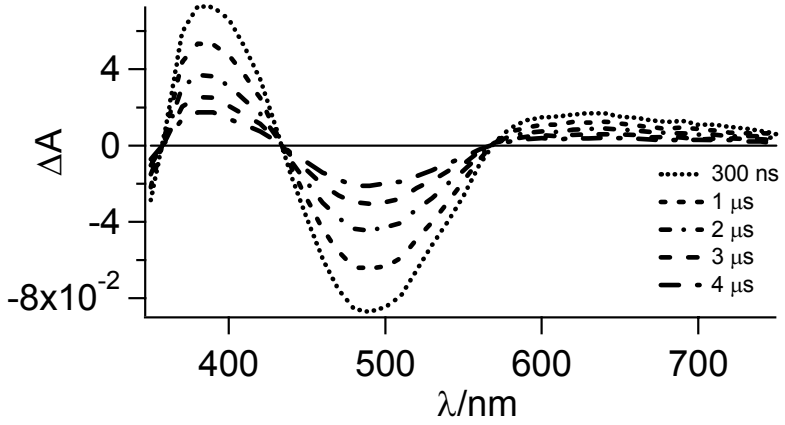

Figure 19. Transient absorption spectrum for $[Ru^{II}(\mathbf{8})_2]^{2+}$ in deoxygenated acetonitrile solution.

To further prove the ^{3}MLCT emission the Zn-complex of ligand **8** was prepared *in situ* and the emission monitored at both room temperature and 77 K, clearly showing different emission wavelengths for the ligand-centered emission and the emission measured in the Ru^{II}-complex.

To summarize this section, the excited state lifetime of Ru^{II}-bis-tridentate complexes can be significantly extended by increasing the bite angles of the ligand so that they are close to octahedral, maintaining a reasonably high excited state energy and keeping a high symmetry of the complex. However, it is also clear from the results discussed in this chapter that the complexes in generation one behave different from the following generations. In order to obtain a deeper understanding of the processes controlling the excited state

decay in the complexes, the temperature dependence of the excited state lifetimes were studied for a number of complexes, two from each generation.

5.5 Excited state deactivation pathways (II-VI)

A detailed analysis of the photophysical results can provide information about the different deactivation pathways involved in the excited state decay. The decay can be divided into two subclasses: radiative and nonradiative decay directly to the ground state, and activated decay processes.

5.5.1 The temperature dependence of the excited state lifetime – identification of activated decay pathways (II, IV, VI)

To gain even more information the temperature dependence of the excited state lifetime can be studied. This was done for two complexes in each generation. The emission lifetime was investigated in the range 80 K up to ambient temperatures, and even higher when possible. Temperature dependent emission lifetime data can be fitted to equation 16 below.[37]

$$\frac{1}{\tau_{obs}} = k_0 + A_1 e^{-\Delta E_1 / RT} + A_2 e^{-\Delta E_2 / RT} + \frac{M}{1 + e^{C(1/T - 1/T_m)}} \tag{16}$$

Included in the constant k_0 are both the radiative and the nonradiative rate constants at liquid nitrogen temperature. The two Arrhenius terms describes activated processes, where the first one is attributed to the thermal equilibrium between the three close lying excited states that constitute the lowest ^{3}MLCT state (described in chapter 4), while the second Arrhenius term corresponds to the thermal activation of the ^{3}MLCT, either as a surface crossing to the ^{3}MC state or an equilibrium with the higher-lying MLCT-state. Finally, the third term in equation 16 is empirical and accounts for the increase in nonradiative decay at the glass-fluid transition of the solvent matrix. This term describes the behavior around a certain temperature, T_m. The parameter C is related to the smoothness of the transition, while M reflects the change as the solvent melts.

The interpretation of the second Arrhenius term deserves a special discussion. Assuming steady state conditions the expression for the observed rate constant will become (equation 17)

$$k_{obs} = \frac{k_1 k_3}{k_2 + k_3} \tag{17}$$

However, when $k_2 << k_3$ the observed rate constant will be equal to k_1 (this means that the decay from the upper state is very rapid) and in this case the overall activation energy E will be equal to the activation energy for process

1, $E(1)$. In this extreme the parameters A_2 and E_2 in the Arrhenius term in equation 16 will correspond to the frequency factor and the activation energy for the surface crossing between the ^{3}MLCT and the upper state. Consequently, for complexes with this behavior, the only way to obtain a long excited state lifetime in fluid solution is to achieve a large activation energy. This is the typical case where surface crossing from the ^{3}MLCT to the ^{3}MC is a dominant pathway. In this case the frequency factor A_2 will be in the range 10^{13}-10^{14} s^{-1}. If the frequency factor is significantly smaller than 10^{13} s^{-1}, it has to be interpreted differently.

In the other extreme, where $k_2>>k_3$ the two states are in equilibrium, since the decay from the upper state is slow compared to the back surface crossing, consequently the observed rate constant will instead become (equation 18)

$$k_{obs}=\frac{k_1 k_3}{k_2} \tag{18}$$

In this case it is not as straightforward to interpret the meaning of the experimentally obtained parameters A_2 and E_2. If the major contribution to the rate constant k_3 comes from a deactivation or reaction process that can be described by an Arrhenius-type relationship, A_2 will correspond the frequency factor of the decay process from the upper state and the activation energy experimentally determined will be the sum of the zero-zero energy difference between the two states and a possible activation energy of the decay process of the upper state. However, if the main contribution to k_3 comes from a non-activated process, the pre-exponential factor will instead be interpreted as the rate of the non-activated upper state decay and the activation energy will be the energy gap between the two states. If the activated decay of the ^{3}MLCT state proceeds via a higher-lying MLCT state, this is the situation and the A_2 parameter does typically fall in the range 10^7-10^8 s^{-1} and thus reflects the lifetime of the upper state.[37] Thus state ordering can be deduced from kinetic analysis of temperature dependent lifetime data. The two cases are schematically depicted in Figure 20.

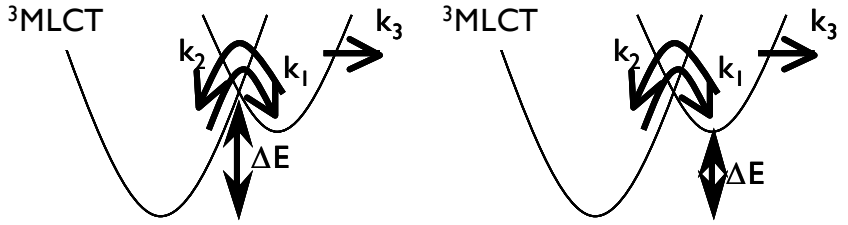

Figure 20. Schematic picture of possible activated pathways for the ^{3}MLCT state. Left: the case where surface crossing is irreversible and ΔE reflects the activation barrier. Right: the case where an equilibrium is established and ΔE reflects the free energy difference between the two states, together with a possible ΔE for k_3.

The temperature dependent lifetime data (markers) and fits to equation 16 (solid lines) are shown in Figure 21 and the parameters from the fits are summarized in Table 7.

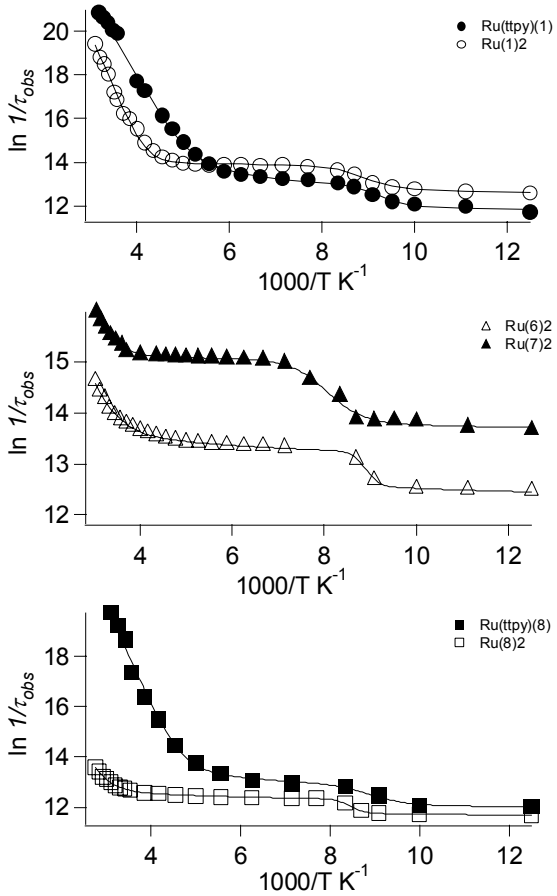

Figure 21. Temperature dependence of the excited state lifetime. Upper panel: First generation $[Ru^{II}(ttpy)(\mathbf{1})]^{2+}$ (open circles), $[Ru^{II}(\mathbf{1})_2]^{2+}$(filled circles). Middle panel: Second generation $[Ru^{II}(\mathbf{6})_2]^{2+}$ (open triangles), $[Ru^{II}(\mathbf{7})_2]^{2+}$ (filled triangles). Lower panel: Third generation $[Ru^{II}(ttpy)(\mathbf{8})]^{2+}$ (filled squares), $[Ru^{II}(\mathbf{8})_2]^{2+}$ (open squares).

As is readily seen from Table 7 and Figure 21, the complexes in the first generation and $[Ru^{II}(ttpy)(\mathbf{8})]^{2+}$ show qualitatively the same temperature dependence and their pre-exponential factors (A_2) can be interpreted as ^{3}MLCT to ^{3}MC surface crossing frequencies. Their activation energies are in the range 2600-3000 cm^{-1} which is significantly higher than the 1500 cm^{-1} for the parent $[Ru^{II}(tpy)_2]^{2+}$. This fact is also reflected in the excited state lifetimes which are significantly longer in all cases. This supports the conclusion that the excited state lifetime can be significantly prolonged by minimizing the interaction between the ^{3}MLCT state and the ^{3}MC state.

Table 7. Parameters from fits to equation 16.

Complex	A_1 /s^{-1}	ΔE_1 /cm^{-1}	A_2 /s^{-1}	ΔE_2 /cm^{-1}	M /s^{-1}	C /K	Tm /K
$[Ru^{II}(ttpy)(\mathbf{1})]^{2+}$	3.8×10^{7}	530	1.6×10^{14}	2600	2.5×10^{5}	3800	110
$[Ru^{II}(\mathbf{1})_2]^{2+}$	4.4×10^{5}	100	1.0×10^{15}	3400	6.9×10^{5}	3700	115
$[Ru^{II}(\mathbf{6})_2]^{2+}$	8.5×10^{5}	230	6.9×10^{9}	1960	2.6×10^{5}	7170	113
$[Ru^{II}(\mathbf{7})_2]^{2+}$	7.2×10^{5}	135	9.2×10^{10}	2200	2.4×10^{6}	2610	128
$[Ru^{II}(ttpy)(\mathbf{8})]^{2+}$	8.2×10^{6}	470	4.7×10^{13}	2700	2.2×10^{5}	2500	115
$[Ru^{II}(\mathbf{8})_2]^{2+}$	3.0×10^{5}	260	1.5×10^{10}	2600	9.9×10^{4}	6200	119

For the complexes in the second generation as well as $[Ru^{II}(\mathbf{8})_2]^{2+}$ the situation is different with A_2 values between 7×10^{9} and 9×10^{10} s^{-1}, and activation energies in the range of 2000 to 2700 cm^{-1}. The pre-exponential factor clearly shows that this is not a ^{3}MLCT - ^{3}MC surface crossing, but rather a situation where equilibrium between with a higher excited state is established. This behavior has been reported for a number of tris-bidentate Ru^{II}-complexes[70, 71, 73] but not for tridentate complexes. The frequency factors reported earlier are in the range 10^7 to 10^8, that is, significantly lower than those obtained for $[Ru^{II}(\mathbf{8})_2]^{2+}$, $[Ru^{II}(\mathbf{6})_2]^{2+}$ and $[Ru^{II}(\mathbf{7})_2]^{2+}$. Another striking difference is that the reported activation energies are all in the range 400 to 1000 cm^{-1} while the bis-tridentate complexes investigated here show significantly higher activation energies. Frequency factors and activation energies in the range 10^{10} s^{-1} have been reported: for $[Ru^{II}(bpy)_2(CN)_2]^{2+}$ and $[Ru(^{II}bpy)(bpyz)_2]^{2+}$ (bpyz = bipyrazine). The explanation offered has been that the reverse surface crossing MC-MLCT would be much faster than the deactivation of the MC state by other routes, so that a pre-equilibrium is set up.[70, 72]

As discussed in paper IV, there are reasons to believe that the activated decay for $[Ru^{II}(\mathbf{6})_2]^{2+}$, $[Ru^{II}(\mathbf{7})_2]^{2+}$ and $[Ru^{II}(\mathbf{8})_2]^{2+}$is not going via a MC state but rather a higher MLCT state, albeit with a much shorter intrinsic lifetime, and thus lower emission quantum yield. There are also reasons to believe that at least some of the few reported cases where a MLCT-MC pre-equilibrium has been previously proposed should be interpreted differently.

5.5.2 Excited state decay rate constants (II-VI)

Once the excited state lifetimes and quantum yields are known the radiative and nonradiative rate constants can be calculated. Rate constants for the activated processes can be calculated from the data obtained from the fit to equation 16 (using the relationship $k = A \times exp(-\Delta E/RT)$). The radiative rate constant is assumed to be essentially temperature independent at temperatures above 77 K. Conversely nonradiative decay is expected to be strongly

activated. At 77 K all activated pathways, except the one via the three close-lying states constituting the lowest ^{3}MLCT state, can be assumed to be turned off and all the nonradiative decay goes directly to the ground state. The calculated rate constants for decay to the ground state and activated processes are summarized in Table 8.

Table 8. Deactivation rate constants at room temperature and 80 K.

Complex	298 K				80 K		
	k_{rad} /s^{-1}	k_{nr}/s^{-1}	k_1/s^{-1}	k_2/s^{-1}	k_{rad}/s^{-1}	k_{nr}/s^{-1}	k_1/s^{-1}
$[Ru^{II}(ttpy)(\mathbf{1})]^{2+}$	1.4×10^5	6.7×10^7	2.9×10^6	5.0×10^8	3.6×10^4	1.1×10^5	7.7×10^3
$[Ru^{II}(\mathbf{1})_2]^{2+}$	7.4×10^4	2.2×10^6	2.7×10^5	6.3×10^7	6.4×10^4	2.4×10^5	1.6×10^4
$[Ru^{II}(\mathbf{6})_2]^{2+}$	6.2×10^3	1.2×10^6	2.8×10^5	5.3×10^5	1.2×10^4	2.3×10^5	1.4×10^4
$[Ru^{II}(\mathbf{7})_2]^{2+}$	1.1×10^4	5.5×10^6	3.8×10^5	2.2×10^6	3.8×10^4	8.0×10^5	6.3×10^4
$[Ru^{II}(ttpy)(\mathbf{8})]^{2+}$	7×10^4	1×10^8	8.5×10^5	1.0×10^8	6×10^4	9×10^4	1.8×10^3
$[Ru^{II}(\mathbf{8})_2]^{2+}$	6×10^3	3×10^5	8.6×10^4	5.3×10^4	7×10^3	1×10^5	2.8×10^3

As can be seen from Table 8 the nonradiative decay directly to the ground state is dominating at low temperatures for all complexes, and all nonradiative rate constants are in the range around 1×10^4 to 2×10^5 s^{-1}. Compared to $[Ru^{II}(bpy)_3]^{2+}$ and $[Ru^{II}(tpy)_2]^{2+}$ these results are unremarkable. The radiative rate constants are in the range 7×10^3 to 7×10^4 s^{-1}. Most strikingly, the radiative rate constants for the two most long-lived complexes are significantly lower than would normally be expected for a Ru^{II}-polypyridine complex.[128] Finally the activated decay to higher lying states is turned off at this temperature, and therefore k_2 is zero (and because of that omitted from Table 8 at 80 K). The rate constant for the activated process between the three close-lying states show, as expected, a higher rate when the energy gap is smaller.

The energy gap law predicts a linear relationship between the logarithm of the nonradiative rate constant and the emission energy and Figure 22 shows this correlation at 80 K. As shown in Figure 22, the homoleptic complexes in the first generation ($[Ru^{II}(\mathbf{1})_2]^{2+}$ and $[Ru^{II}(\mathbf{5})_2]^{2+}$) deviates significantly from the others. This can be explained by their closer similarity with bipyridine than with terpyridine complexes, as judged from the distortion between ground and excited state nuclear geometry. However, the number of data points in each generation is not enough to conclude if the relationship is valid or not for the complexes investigated.

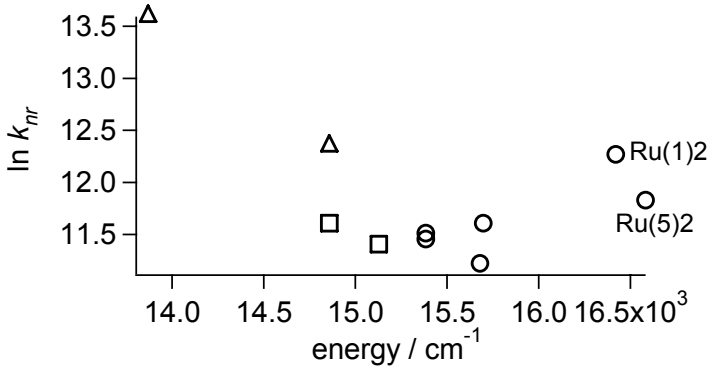

Figure 22. Correlation between the logarithm of the nonradiative rate constant at 80 K and the emission energy. Circles: first generation, triangles: second generation, and squares: third generation.

Activated decay via MC states is the dominating process for the complexes in the first generation at room temperature, as is the case for for both $[Ru^{II}(bpy)_3]^{2+}$ and $[Ru^{II}(tpy)_2]^{2+}$.[37] However, compared to $[Ru^{II}(tpy)_2]^{2+}$ the deactivation rate is reduced with one and two orders of magnitude, clearly indicating that the activation barrier for decay via ^{3}MC states are significantly higher and that our strategy is working. In contrast, for the second generation, the excited state decay at room temperature is not dominated by an activated process, but by direct nonradiative decay to the ground state. For $[Ru^{II}(\mathbf{7})_2]^{2+}$ this effect can be attributed to its very low excited state energy and consequently a larger nonradiative decay rate constant, but this cannot explain the results for $[Ru^{II}(\mathbf{6})_2]^{2+}$. The fact that the decay is not dominated by an activated process suggests that the energy gap to the ^{3}MC state must be significantly higher than in $[Ru^{II}(tpy)_2]^{2+}$.

Finally, in the third generation, the two complexes behave differently. For the heteroleptic complex the nonradiative decay and the activated decay are in the same order of magnitude, and several orders of magnitude higher than the radiative decay. For the homoleptic complex on the other hand, the dominating rate constant at room temperature is once again the nonradiative decay rate constant. Here the activation energy is even higher than for the complex in the second generation, and hence the activation barrier for decay via a ^{3}MC state even higher.

To summarize this section it can be concluded the applied design strategy do result in improved photophysical properties *e.g.* increased emission quantum yields, longer excited state lifetimes and still reasonably high excited state energies. Moreover, it is shown that the increase in excited state lifetime is due to a substantial reduction of the nonradiative decay rate. It can also be concluded that the microsecond MLCT excited state lifetimes observed cannot be explained only by a decrease of the excited state energy. Finally, the third generation can be symmetrically substituted with electron

donor and acceptor motifs giving the possibility of rod-like molecular arrays: It can thus be concluded that the strategy has been proved successful.

5.6 Localization of the excited state (II, III, VI, VII)

In mixed ligand complexes it is, as discussed in chapter 4.7, very important to control on which of the ligands the lowest excited state is localized, since this can change the photophysical properties significantly. This is even more important when an electron acceptor is attached, since electron transfer efficiency will be dramatically affected depending on where the excited state is localized.[21, 86, 87] The excess electron density of the excited state is localized on the ligand easiest to reduce.[37, 50] Another aspect of excited state localization is that not all ligands are chromophoric, or may have very different chromophoric properties, as can be seen in complex $[Ru^{II}(ttpy)(\mathbf{8})]^{2+}$ and $[Ru^{II}(\mathbf{8})_2]^{2+}$. This implies that slight structural modifications can be used to switch an emissive complex into a non-emissive or vice versa.

Another interesting approach to linear **D-P-A**-arrays is, instead of using tridentate ligands, to attach both the donor and the acceptor on different sides of the same ligand, thus creating a linear array with separation in space between the donor and the acceptor motifs, Figure 23. This approach is especially interesting for tris-bidentate complexes. Furthermore this approach may offer a possibility to do "on-complex" functionalization which can be useful.

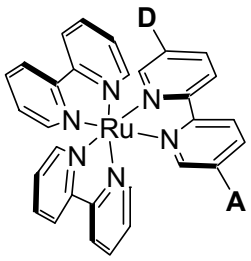

Figure 23. Schematic picture describing the possibility of constructing linear donor-acceptor arrays with tris-bidentate complexes.

5.6.1 Modulation of the lowest excited state by small changes in ligand structure – A case study (VII)

One example of two complexes that differ only slightly from the structural point of view but still have very different emission properties are shown in Figure 24.

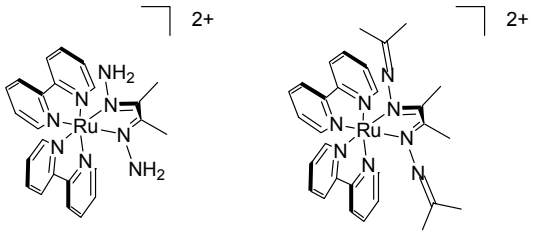

Ru(bpy)$_2$(**9**) Ru(bpy)$_2$(**10**)

Figure 24. Structure of the complexes investigated in this study. Note the small structural difference between the complexes.

The electronic absorption spectra of the two complexes are shown in Figure 25. The UV part is dominated by the π-π* transition of the bpy ligands, centered around 288 nm and both exhibit the expected MLCT-transition in the 400-500 nm spectral region. Even though the maximum absorption is blue-shifted in $[Ru^{II}(bpy)_2(\mathbf{9})]^{2+}$**,** and the molar absorptivity is slightly lower the differences are not large enough to expect big differences in emission properties. $[Ru^{II}(bpy)_2(\mathbf{9})]^{2+}$ is completely non-emissive even at 77 K, while $[Ru^{II}(bpy)_2(\mathbf{10})]^{2+}$ exhibits appreciable emission both at room temperature and low temperature. The excited state lifetime of $[Ru^{II}(bpy)_2(\mathbf{10})]^{2+}$ at room temperature is 42 ns and the emission quantum yield is 2×10^{-3}. At 80 K however, the emission quantum yield and excited state lifetime are 7×10^{-3} and 178 ns respectively. Ru^{II}-polypyridine complexes normally have lifetimes between 1 and 15 μs in solid matrix at liquid nitrogen temperature, although they may be very short-lived at room temperature (less than 1 ns). The radiative rate constant however is almost temperature-independent and falls in the same range as for many other Ru^{II}-polypyridine complexes. Thus, even though the excited state lifetime and the emission quantum yield at 80 K is much lower than normally expected, these results are not conclusive concerning which ligand is involved in the lowest excited state.

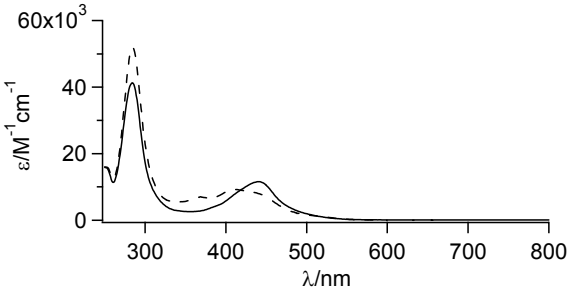

Figure 25. Absorption spectra for $[Ru(bpy)_2(\mathbf{9})]^{2+}$ (dashed line) and $[Ru(bpy)_2(\mathbf{10})]^{2+}$ (solid line).

Electrochemical measurements reveal irreversible oxidations at 1.23 V and 1.29 V (vs NHE) for $[Ru^{II}(bpy)_2(\mathbf{9})]^{2+}$ and $[Ru^{II}(bpy)_2(\mathbf{10})]^{2+}$ respectively, and reductions at –1.13 and – 1.11 V. From these data it is not possible to attribute the first reduction to a specific ligand moiety in any of the complexes. From comparison with $[Ru^{II}(bpy)_3]^{2+}$ measured under the same conditions it is clear that the LUMO's in $[Ru^{II}(bpy)_3]^{2+}$ and the cations of $[Ru^{II}(bpy)_2(\mathbf{9})]^{2+}$ and $[Ru^{II}(bpy)_2(\mathbf{10})]^{2+}$ are quite close in energy. It is not possible to determine which ligand is the most easily reduced in $[Ru^{II}(bpy)_2(\mathbf{9})]^{2+}$ and $[Ru^{II}(bpy)_2(\mathbf{10})]^{2+}$ just from the redox data above.

Spectroelectrochemistry was performed on both complexes, in order to elucidate which ligand that is reduced first in each of the complexes. Difference spectra (final – initial) for both complexes are given in Figure 26. Although they may seem very similar at first sight, important differences appear at closer inspection. First, the peak at 288 nm displays an electrochromic shift for both complexes, but the intensity is almost unchanged for $[Ru^{II}(bpy)_2(\mathbf{9})]^{2+}$ but decreases in $[Ru^{II}(bpy)_2(\mathbf{10})]^{2+}$, to almost two thirds of its initial intensity. This behavior is consistent with a reduction of one of the bpy ligands in $[Ru^{II}(bpy)_2(\mathbf{10})]^{2+}$. Second, the band appearing at 360 nm in $[Ru^{II}(bpy)_2(\mathbf{10})]^{2+}$ is typical for a reduced bipyridine and its position is generally independent of the identity of the other ligands in the complex. The corresponding feature in $[Ru^{II}(bpy)_2(\mathbf{9})]^{2+}$ is instead shifted to the blue. Third, the bleaching of the MLCT band is present in both complexes, but is more pronounced for $[Ru^{II}(bpy)_2(\mathbf{10})]^{2+}$, indicating a bleach of a relatively strong $Ru^{II} \rightarrow$ bpy transition in $[Ru^{II}(bpy)_2(\mathbf{10})]^{2+}$, but a weaker $Ru^{II} \rightarrow$ dihydrazone transition in $[Ru^{II}(bpy)_2(\mathbf{9})]^{2+}$. Finally, the spectrum of $[Ru^{II}(bpy)_2(\mathbf{10})]^{2+}$, exhibits an absorption band around 510 nm identical to the band for reduced $[Ru^{II}(bpy)_3]^{2+}$.[129]

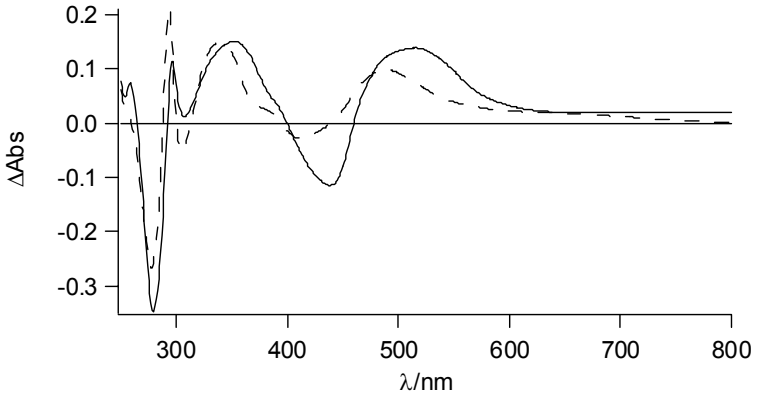

Figure 26. Difference spectra for $[Ru^{II}(bpy)_2(\mathbf{9})]^{2+}$ (dashed line) and $[Ru^{II}(bpy)_2(\mathbf{10})]^{2+}$ (solid line).

To gain further evidence for a bpy ligand being first reduced in $[Ru^{II}(bpy)_2(\mathbf{10})]^{2+}$, transient absorption measurements were performed in the spectral range 350-800 nm. The resulting transient spectrum is very similar to that of $[Ru^{II}(bpy)_3]^{2+}$, and displays all the well known spectral features of a reduced bpy-ligand. The decay time constant is uniform over the whole spectral range, and the same as the excited state lifetime. In particular, the excited state absorption around 360 nm and the isosbetic point at 400 nm suggest that the lowest ^{3}MLCT state in $[Ru^{II}(bpy)_2(\mathbf{10})]^{2+}$ is indeed localized on a bpy moiety.[127]

From the spectroelectrochemistry and transient absorption it can be concluded that in $[Ru^{II}(bpy)_2(\mathbf{10})]^{2+}$, a bpy ligand is easiest to reduce and that implies that the lowest ^{3}MLCT is localized on one of the bpy ligands. By constrast, the ligand easiest to reduce in $[Ru^{II}(bpy)_2(\mathbf{9})]^{2+}$ is the dihydrazone moiety, and as a consequence, the lowest ^{3}MLCT state is localized on the same ligand.

The fact that the lowest ^{3}MLCT state is of different nature in the two complexes can explain the large differences in photophysical properties. It is also evident that a structural modification of the ligand that may appear very small can be accompanied by large differences in photophysical behavior of the corresponding complexes.

5.7 Towards predictive power? (III, V, VI, VIII)

The number of ligands that can be used in a Ru^{II}-based photosensitizer is immense. To synthesize and experimentally characterize them all are time consuming and expensive, and therefore it would be valuable to somehow be able to predict the absorption and excited state properties, and in particular the excited state lifetime, of Ru^{II}-polypyridyl complexes. Computational

methods such as molecular mechanics (MM) and density functional theory (DFT) provide structural predictions and time dependent DFT (TD-DFT) also spectral properties. However, there is no method to computationally arrive directly at the excited state lifetime. In order to evaluate the possibility of finding a theoretically available parameter that could somehow be related to and indirectly predict the excited state lifetime, computational studies were undertaken.

5.7.1 Structural predictions

The singlet ground state geometry can be predicted either with MM calculations or with DFT. MM calculations with an appropriate parameterization often give structures that are in good agreement with experimentally obtained crystal structures. However, DFT at the B3LYP/LANL2DZ level of theory seems to give more accurate results when several possible conformations are close in energy. In general, DFT gives structural predictions that are in good agreement with crystal structures, although Ru-N bond lengths are slightly overestimated.

Since the coordination geometry of a complex is important for its photophysical properties the fifteen N-Ru-N angles are of particular interest. If they deviate too much from the ideal 180° or 90°, the complex is not very octahedral. One attempt was to establish an octahedricity measure, based on the angular deviation from ideal octahedral coordination of all the fifteen N-Ru-N angles. Deviations between 0.5° for the model complex $[Ru^{II}(py)_6]^{2+}$ and 3° for $[Ru^{II}(tpy)_2]^{2+}$ were observed. $[Ru^{II}(py)_6]^{2+}$ can be expected to be very close to octahedral since every pyridine is monodentate with a minimum steric restriction. However, according to this measure the most octahedral of the complexes investigated is actually $[Ru^{II}(\mathbf{8})_2]^{2+}$ giving a deviation of only 0.4° (papers V, VI, VIII)

5.7.2 Spectral predictions

Spectral predictions can be made with TD-DFT methods. The overall agreement between the simulated absorption spectra (at the TD-B3LYP/LANL2DZ level) and experimentally obtained results is good for unsubstituted Ru^{II}-polypyridyl complexes, but some discrepancies are seen in the visible region of the spectrum. For a majority of the investigated complexes the MLCT absorption is reproduced within 20 nm of its experimental value, but often energetically overestimated. An example of the agreement is shown in Figure 27.

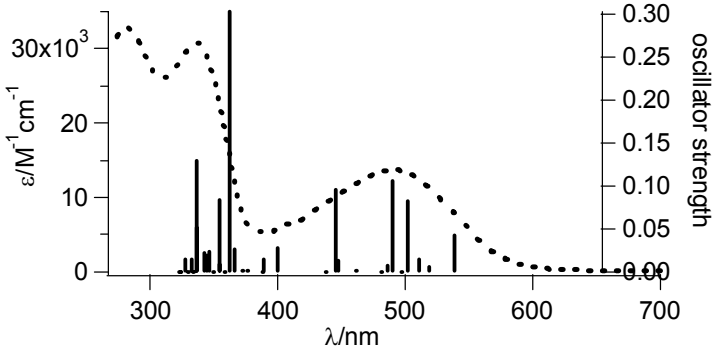

Figure 27. Comparison of experimentally obtained and TD-DFT calculated absorption spectrum for $[Ru^{II}(\mathbf{8})_2]^{2+}$. Dotted line: experiment, and bars: calculations.

5.7.3 Energetic predictions (III)

Another computational possibility is to locate the actual structures and relative energies of the ground state, the ^{3}MLCT and ^{3}MC states and thereby establish an energetic relationship between them. Using this approach, it is possible to construct energy diagrams for the complexes, and thus be able to estimate the ^{3}MLCT – ^{3}MC barrier for thermal deactivation from the ^{3}MLCT state. The diagrams are constructed from the total energy of the optimized states, the vertical single-point energies of the ground state surface for the ^{3}MLCT and ^{3}MC geometries and vertical singlet and triplet excitation energies of the ground state.

The results for $[Ru^{II}(\mathbf{1})_2]^{2+}$ and $[Ru^{II}(\mathbf{5})_2]^{2+}$ are qualitatively in agreement with experimentally obtained results, and it is noteworthy that in $[Ru^{II}(\mathbf{5})_2]^{2+}$ the calculated ^{3}MC state is actually lower in energy than the ^{3}MLCT state, and since also the activation barrier is low, the very short excited state lifetime observed is not surprising.

5.7.4 A parameter for the excited state lifetime?

The d-d splitting, Δ_O, can be extracted from the energy difference between the highest occupied t_{2g} orbital and the lowest unoccupied e_g orbital in the electronic structure. The magnitude of the d-d splitting is dependent on the octahedricity of the complex, but also on the distance between the ligand and the ruthenium core. For example $[Ru^{II}(py)_6]^{2+}$ has a very octahedral coordination as expected by the highly flexible ligands, but still the d-d splitting is relatively small. However, the calculations indicate a correlation between the experimentally obtained excited state lifetimes and the calculated d-d split-

ting, such that a small increase in the d-d energy difference over 6 eV (calculated at the B3LYP/LANL2DZ level) appears to result in a large increase of excited state lifetime. Nevertheless, more extensive studies are needed to establish a general relationship of this kind.

5.7.5 Overall predictive power?

It is clear that calculations can provide good structural prediction, at least for ground state geometries. Also, spectral prediction is possible with reasonable agreement with experiments. Establishment of a direct correlation between a parameter computationally available and the excited state lifetime is yet not possible, although there are indications of qualitative agreement. Although the structures and energetics of the relevant ground and triplet states can be calculated, calculations can presently not describe all the processes important for the excited state lifetime. Nevertheless it can be concluded that calculations can give interesting insights and predictions of the properties of a specific complex, although the overall predictive power needs further improvements.

6 Conclusions and future outlook

The main theme of this thesis is tuning of the excited state properties of Ru^{II}-polypyridyl complexes, and more specifically to prolong the excited state lifetime of bis-tridentate complexes, without a concomitant decrease of the excited state energy. Since many attempts to increase the excited state lifetime of bis-tridentate Ru^{II}-complexes have resulted in a substantial lowering of the excited state energy, thus also reducing its reactivity, a new strategy to extend the excited state lifetime was outlined, investigated and proven to be successful.

The strategy is based on the idea that a more octahedral coordination can destabilize the metal e_g orbitals, thus leading to a higher energy for the ^{3}MC state which is responsible for a large part of the room temperature nonradiative decay of tris-bidentate Ru^{II}-complexes in general. This would lead to a slower transition from the emissive ^{3}MLCT to the ^{3}MC states, resulting in the desired longer lifetime of the ^{3}MLCT state.

In our first generation of photosensitizers, a 50-fold increase of the excited state lifetime, compared to the parent $[Ru^{II}(tpy)_2]^{2+}$ was obtained, clearly showing that ligands with better bite angles, *i.e.* more close to octahedral, induce a destabilization of the ^{3}MC energy and thus give longer excited state lifetimes. A second generation of photosensitizers resulted in even longer excited state lifetimes. Finally, the third generation of photosensitizers resulted in a close to octahedral coordination, and excited state lifetimes in the microsecond region, which is an increase of around four orders of magnitude compared to the parent Ru^{II}-bis-terpyridine complex. Furthermore, the complexes in the third generation allows for symmetric substitution that can be used for construction of linear supramolecular assemblies.

An obvious future step is to construct **P-A** and **D-P** dyads and to prove that the desired electron transfer reactions can occur also in a linked system. Once this has been shown a second step would be to construct linear **D-P-A** arrays based on the third generation of photosensitizers.

If the favorable photophysical properties of the photosensitizers in the third generation can be maintained upon covalent attachment of electron donor and acceptor motifs, the possible use of these rod-like arrays are not restricted to artificial photosynthesis applications but can also be interesting for other areas such as molecular electronics and switches.

7 Experimental techniques

The photophysical properties of transition metal complexes can be studied with different steady state and time-resolved spectroscopic techniques. Interesting excited state dynamics can be probed both by emission and by transient absorption measurements. Electrochemical techniques can be used to reveal important thermodynamic information about the systems. Furthermore, combinations of spectroscopic and electrochemical techniques can be used to identify and characterize intermediates and products of a redox reaction.

7.1 Spectroscopic techniques

Emission spectroscopy provides a direct measure of the radiative decay from the electronically excited state, caused by a photon hitting the sample molecules. Absorption spectroscopy can be performed on the sample in its ground state, but also probe the excited state, by first exciting the sample with a laser flash. The transient absorption signal can be expressed as (equation 19)

$$\Delta A = -\lg(I_{ES} / I_{ref}) - (-\lg(I_{GS} / I_{ref})) = \lg(I_{GS} / I_{ES}) \quad (19)$$

there I_{GS}, I_{ES} and I_{ref} are the intensities of the light beam after it has passed the sample in its ground state, in its excited state and after passing a reference medium not containing the sample, respectively.

7.1.1 Steady state emission spectroscopy

Steady state emission measurements are performed with the sample held under constant irradiation by a white light source, *i.e.* a Xe-lamp. A specific excitation wavelength is obtained by the use of a monochromator. The sample absorbs the light and the emitted photons are detected at right angle to the excitation light. The emission is focused on the entrance slit of a second, scanning, monochromator and detected with a photomultiplier tube (PMT).

7.1.2 Flash photolysis

Time-resolved emission and transient absorption dynamics slower than ca 20 ns can be probed with a flash photolysis set-up. A frequency-tripled Q-switched Nd:YAG laser, producing laser flashes with a width of <10 ns is used for excitation. The excitation laser light, tunable between 410 and 680 nm, is produced in an optical parametric oscillator, OPO. In the case of transient absorption, the analyzing light comes from a 150W Xe-lamp irradiating the sample after excitation with the laser beam. For emission as well as transient absorption measurements, the signal is passed through a monochromator and detected at right angle to the excitation light with a photomultiplier tube, PMT. The PMT output is recorded with a digital oscilloscope and converted to readable data before transfer to a computer. A schematic picture of the system is shown in Figure 28.

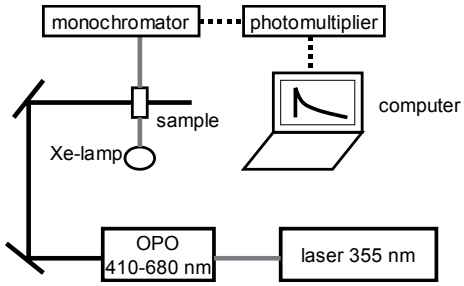

Figure 28. Schematic picture of the flash photolysis experimental set up.

7.1.3 Time-correlated single photon counting

Time-correlated single photon counting is a statistical method used to record time-resolved emission slower than ~10 ps, Figure 29.

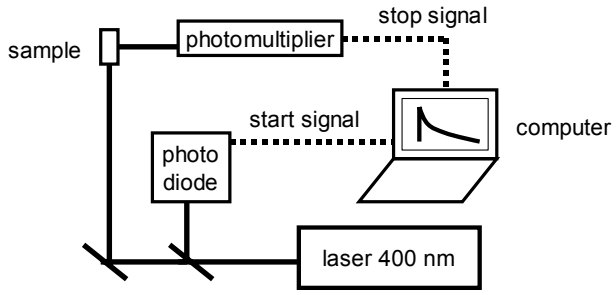

Figure 29. Schematic picture of the single photon counting experimental set up.

Only one photon at a time is collected by the detector. Light pulses at 400 nm, and with a pulse repetition frequency of 200 kHz, irradiate the sample. The emission is detected at right angle to the excitation light, by a microchannel plate photomultiplier. To prevent scattered light from reaching the detector, filters are placed between the sample and the detector. Since the method is statistical the pump light intensity must be weak enough so that only one photon hits the photomultiplier during the experimental time window. The time difference between the arrival of this photon and the arrival of the light pulse is detected by a photodiode. By the collection of a large number of data points a histogram of hits versus time can be constructed.

7.2 Electrochemical techniques

Electrochemical techniques give a good overview of the redox processes occurring within a certain potential range. Cyclic voltammetry can be used to determine thermodynamic properties for electrochemical reactions, as well as study the kinetics of the same reaction. A cyclic voltammogram give the potential at which a charge-transfer reaction occur, and indicates if the process is reversible or not. A three-electrode system, consisting of a working electrode (where the reaction takes place), a reference electrode (with a constant potential) and counter electrode (through which large currents can pass) and a potentiostat are needed. The potentiostat applies the desired potential between the working and the reference electrodes. Cyclic voltammetry (CV) is performed by cycling the potential of the working electrode, and meanwhile detect the resulting current. In differential pulse voltammetry (DPV) the potential is pulsed instead of varied linearly. Chronoamperometry is used for bulk electrolysis. A potential is applied on the working electrode for a long time to convert all the redox active species in the solution.

7.3 Spectroelectrochemistry

Electrochemistry and spectroscopy can be combined into the powerful spectroelectrochemistry technique. Spectroscopic detection occurs simultaneously with the electrochemical reduction or oxidation, and so can the spectrum of the oxidized or reduced species be detected. The actual potential is chosen from DPV or CV measurements and chronoamperometry is the method most commonly used for electrolysis of the sample. The spectral changes are detected during the electrolysis and so intermediates and products of a redox reaction can be studied spectroscopically.

Acknowledgements

Many people have been involved in this work, one way or another and, I´d like to acknowledge…

…My advisors Leif Hammarström and Hans-Christian Becker. For being good supervisors, for inspiration, motivation, support, sharing of ideas and many interesting discussion on things like chemistry, politics, gender issues and more…

…All past and present CAP-members. No one mentioned, no one forgotten.

…All collaborators and co-authors. Olof Johansson, Henriette Wolpher and Michael Jäger for providing me with pure complexes and Maria Lundqvist, Anders Borg and Petter Persson for a nice collaboration. My diploma and summer students; Jan Larsson, Erik Göransson & Tomas Österman for good work and good mood.

…All past and present colleagues at both Fysikalen and Fotomol. For a nice time and for encouragement and help whenever needed. Especially Reiner Lomoth for helping out with electrochemistry. Special thanks also to you who helped out with things like references, figures, encouragement etc, during the last days of writing. And to all of you: Don´t work too much! ☺

…Daniel Karlsson, Mattias Eklund, Paulo Oliveira, Mats Fröberg, Staffan Wallin and Maria Lundqvist for proof reading earlier versions of this thesis.

…Karin Stensjö, Malin Abrahamsson and Kristine Kilså: support, encouragement and advice have been much appreciated!

…Family and all friends! Especially the people at my recreation facilities at Udden and Kolugnsvägen – Tryggve & Andrea, Maria & Per, Mats for always believing in me and Johan, Jenny, Sara B. and Sus for always being there.

Finally, without help, support and concern from Maria and Mattias, I don´t know how (or even if) I would have managed to finish this. Tack för allt!

Summary in Swedish

Artificiell fotosyntes – Att göra bränsle av sol och vatten

Vem som helst som har varit i en storstad på natten inser att mänskligheten förbrukar stora mängder energi bara på att lysa upp omgivningen: Och det handlar ändå bara om en liten del av all den energi som det moderna samhället behöver. I en tid när klimatfrågan klassas som en av de viktigaste framtidsfrågorna och det debatteras hur länge oljan kommer att räcka borde vår energiförbrukning stämma till eftertanke. Vi behöver en ny, miljövänlig energikälla. Så frågan är var vi ska leta?

På en timme strålar solen in mer energi till jorden än vad mänskligheten förbrukar under ett helt år. Om vi kan lära oss att samla upp och utnyttja bara en bråkdel av den energin har vi lösningen på framtidens energiförsörjningsproblem. Det vore inte bara dumt, utan också oansvarigt att inte undersöka potentialen i solen som energikälla.

För att läsa oss omvandla solljus till kemisk energi hämtar vi inspiration från naturen själv, där växterna redan gör det mänskligheten ännu inte klarar. I fotosyntesen utnyttjas solenergin för att göra det bränsle som växterna behöver, såsom ATP och NADPH. Detta är den process som står modell för den forskning som bedrivs inom ramen för det svenska konsortiet för artificiell fotosyntes, forskning med det slutgiltiga målet att göra bränsle av solenergi och vatten.

För att kunna härma de viktiga stegen och nyckelreaktionerna krävs en detaljerad förståelse av alla de olika komplicerade processer som ingår i fotosyntesen. Solljuset fångas in av antenner, klorofyllmolekyler, som sedan överför energin till en uppsättning molekyler där själva reaktionerna sker. I detta s.k. reaktionscentrum finns en särskild sorts molekyler som tar emot den uppsamlade energin i solljuset. Dessa molekyler kallas fotosensiterare.

När fotosensiteraren tar emot energin från solljuset blir molekylen exciterad, det vill säga att den antar ett högre energitillstånd. Den exciterade molekylen kan antingen avge denna extra energi genom att sända ut ljus eller värme, eller genom att ge en elektron till en angränsande molekyl – en elektronacceptor. Den senare processen är den önskade och leder till ett ladd-

ningsseparerat tillstånd. Det innebär att det finns en extra elektron hos acceptorn medan fotosensiteraren saknar en elektron. För att återställa fotosensiteraren tar den en elektron från ett mangankluster som katalyserar elektronöverföringsreaktionen.

När excitationen och elektronöverföringsprocessen har skett fyra gånger oxiderar mangankomplexet två vattenmolekyler till syrgas och protoner. Detta sista steg låter enkelt men är i själva verket det mest magiska av alla steg i fotosyntesen. Om vi kan lära oss att härma alla dessa reaktioner kan vi, genom vattenoxidation, få fram protoner som sedan kan reduceras till vätgas, som är en utmärkt energibärare och som det finns utvecklad teknik för att använda som bränsle. Det är dock fortfarande långt kvar innan vi kan göra en molekyl som klarar av att härma alla dessa steg.

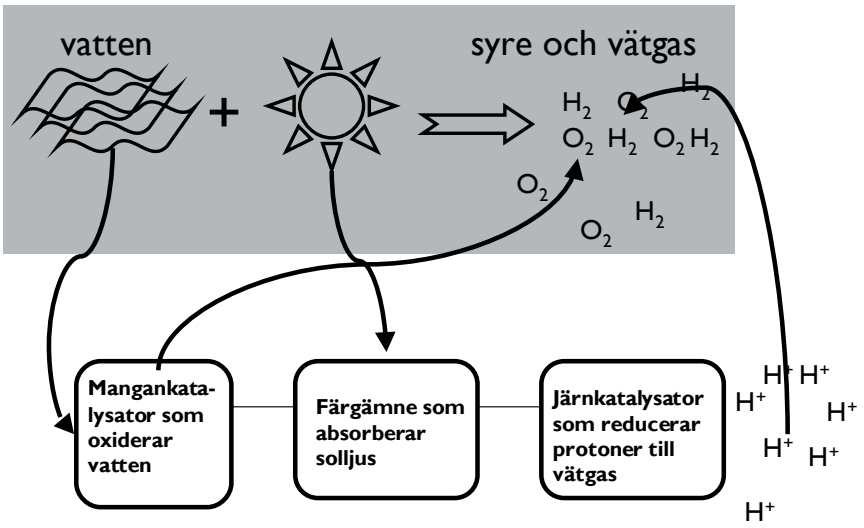

Figur 30. Schematisk bild av ett artificiellt fotosyntessystem.

Min avhandling handlar om att studera de för artificiell fotosyntes kritiska egenskaperna hos molekyler som är avsedda att härma naturens klorofyll i reaktionscentrat, det vill säga fotosensiteraren (färgämnet). Istället för att använda klorofyll, som inte är särskilt stabilt, har vi använt föreningar som innehåller metallen rutenium. För att dessa ska fungera krävs att de är stabila, att de absorberar mycket synligt ljus, och att de exciterade tillstånd som bildas när ljuset tas upp är tillräckligt långlivade för att de övriga önskade reaktionerna ska hinna ske. Utöver detta måste de exciterade tillstånden vara tillräckligt energirika för att driva elektrontransporten som ger det laddningsseparerade tillståndet. Fotosensiteraren bör också ha sådan struktur att det är möjligt att länka electronacceptorn och manganklustret till fotosensiteraren så att de sitter på motsatta sidor om ruteniumkomplexet. Genom en sådan

geometri förenklas konstruktionen av stora komplex och risken för oönskade reaktioner minskas.

I avhandlingen presenteras ett antal nya ruteniumkomplex med förbättrade fotofysiska och geometriska egenskap. Komplexens detaljerade fotofysik har studerats med avseende på egenskaper som effektivitet för ljusabsorption, det exciterade tillståndets energi och livslängd.

Arbetet med att ta fram förbättrade molekyler har skett i flera steg och resulterat i ett flertal förbättringar. I ett första steg förlängde vi det exciterade tillståndets livslängd 50 gånger, till 15 ns (0.000 000 015 s). Sedan har vi genom en kombination av experiment och teori gått vidare och åstadkommit ytterligare förbättringar till 800 ns (0.000 000 8 s) och som bästa resultat har vi en molekyl vars exciterade tillstånd är stabilt i 3 mikrosekunder (0.000 003 s), vilket är en klar förbättring jämfört med tidigare resultat.Från detta komplex, som är det modellkomplex som har den hittills kända längsta livslängden hos ett ruteniumkomplex, har vi också visat att det är möjligt att inkorporera dem i större system för att driva de önskade elektronöverföringsreaktionerna. Min forskning löser inte energiproblemen, men är ett litet steg på vägen mot ett framtida hållbart energisystem.

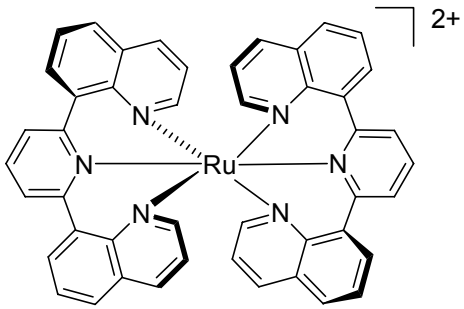

Figur 31.Ruteniumkomplexet som har ett exciterat tillstånd som lever i tre mikrosekunder.

References

1. *World energy assessment: energy and the challenge of sustainability*, J. Goldemberg, Editor. 2000, United Nations Development Programme/ United Nations Department of Economic and Social Affairs, World Energy Council: New York.
2. Lewis, N.S.; Nocera, D.G. *PNAS* **2006**, *103,* 15729-15735.
3. Hagfeldt, A.; Gratzel, M. *Acc. Chem. Res.* **2000**, *33,* 269-277.
4. Gratzel, M. *J. Photochem. Photobiol. C* **2003**, *4,* 145-153.
5. Kazmerski, L.L. *J. Elect. Spect. Rel. Phen.* **2006**, *150,* 105-135.
6. Alstrum-Acevedo, J.H.; Brennaman, M.K.; Meyer, T.J. *Inorg. Chem.* **2005**, *44,* 6802-6827.
7. Barber, J. *Quarterly Reviews of Biophysics* **2003**, *Volume 36,* 71-89.
8. Buchanan, B.E.; Gruissem, W.; Jones, R.L., *Biochemistry and molecular biology of plants*. 2000, Rockville: American Society of Plant Physiologists.
9. Debus, R.J.; Barry, B.A.; Sithole, I.; Babcock, G.T.; McIntosh, L. *Biochem.* **1988**, *27,* 9071-9074.
10. Rupprecht, J.; Hankamer, B.; Mussgnug, J.H.; Ananyev, G.; Dismukes, C.; Kruse, O. *App. Microbiol. Biotech.* **2006**, *72,* 442-449.
11. Tamagnini, P.; Axelsson, R.; Lindberg, P.; Oxelfelt, F.; Wunschiers, R.; Lindblad, P. *Microbiol. Mol. Bio. Rev.* **2002**, *66,* 1-+.
12. Nishitani, S.; Kurata, N.; Sakata, Y.; Misumi, S.; Karen, A.; Okada, T.; Mataga, N.; Negue, M.A. *J. Am. Chem. Soc.* **1983**, *105,* 7771-7772.
13. Moore, T.A.; Gust, D.; Mathis, P.; Mialocq, J.-C.; Chachaty, C.; Bensasson, R.V.; Land, E.J.; Doizi, D.; Liddell, P.A.; Lehman, W.R.; Nemeth, G.A.; Moore, A.L. *Nature* **1984**, *307,* 630-632.
14. Wasielewski, M.R.; Niemczyk, M.P.; Svec, W.A.; Pewitt, E.B. *J. Am. Chem. Soc.* **1985**, *107,* 5562-5563.
15. Danielson, E.; Elliott, C.M.; Merkert, J.W.; Meyer, T.J. *J. Am. Chem. Soc.* **1987**, *109,* 2519-2520.
16. Meyer, T.J. *Acc. Chem. Res.* **1989**, *22,* 163-170.
17. Sun, L.C.; Hammarstrom, L.; Akermark, B.; Styring, S. *Chem. Soc. Rev.* **2001**, *30,* 36-49.
18. Hammarstrom, L. *Curr. Op. Chem. Biol.* **2003**, *7,* 666-673.
19. Lomoth, R.; Magnuson, A.; Sjodin, M.; Huang, P.; Styring, S.; Hammarstrom, L. *Photosynt. Res.* **2006**, *87,* 25-40.
20. Berglund-Baudin, H.; Sun, L.C.; Davidov, R.; Sundahl, M.; Styring, S.; Akermark, B.; Almgren, M.; Hammarstrom, L. *J. Phys. Chem. A* **1998**, *102,* 2512-2518.

21. Abrahamsson, M.L.A.; Baudin, H.B.; Tran, A.; Philouze, C.; Berg, K.E.; Raymond-Johansson, M.K.; Sun, L.C.; Akermark, B.; Styring, S.; Hammarstrom, L. *Inorg. Chem.* **2002**, *41,* 1534-1544.
22. Huang, P.; Magnuson, A.; Lomoth, R.; Abrahamsson, M.; Tamm, M.; Sun, L.; Rotterdam, B.v.; Park, J.; Hammarström, L.; Åkermark, B.; Styring, S. *J. Inorg. Biochem.* **2002**, *91,* 159-172.
23. Rüttinger, W.; Dismukes, G.C. *Chem. Rev.* **1997**, *97,* 1 - 24.
24. Mukhopadhyay, S.; Mandal, S.K.; Bhaduri, S.; Armstrong, W.H. *Chem. Rev.* **2004**, *104,* 3981-4026.
25. Yagi, M.; Kaneko, M. *Chem. Rev.* **2001**, *101,* 21-35.
26. Borgström, M.; Johansson, O.; Lomoth, R.; Berglund-Baudin, H.; Wallin, S.; Sun, L.; Åkermark, B.; Hammarström, L. *Inorg. Chem.* **2003**, *42,* 5173-5184.
27. Johansson, O.; Borgström, M.; Lomoth, R.; Palmblad, M.; Bergquist, J.; Hammarström, L.; Sun, L.; Åkermark, B. *Inorg. Chem.* **2003**, *42,* 2908-2918.
28. Rauchfuss, T.B. *Inorg. Chem.* **2004**, *43,* 14-26.
29. Evans, D.J.; Pickett, C.J. *Chem. Soc. Rev* **2003**, *32,* 268-275.
30. Ott, S.; Kritikos, M.; Akermark, B.; Sun, L.C.; Lomoth, R. *Angew. Chem. Int. Ed.* **2004**, *43,* 1006-1009.
31. Ott, S.; Borgstrom, M.; Kritikos, M.; Lomoth, R.; Bergquist, J.; Akermark, B.; Hammarstrom, L.; Sun, L.C. *Inorganic Chemistry* **2004**, *43,* 4683-4692.
32. Wolpher, H.; Borgstrom, M.; Hammarstrom, L.; Bergquist, J.; Sundstrom, V.; Stenbjorn, S.; Sun, L.C.; Akermark, B. *Inorg. Chem. Commun.* **2003**, *6,* 989-991.
33. Wallin, S.; Hammarstrom, L.; Blart, E.; Odobel, F. *Photochem. Photobiol. Sci.* **2006**, *5,* 828-834.
34. Borgstrom, M.; Blart, E.; Boschloo, G.; Mukhtar, E.; Hagfeldt, A.; Hammarstrom, L.; Odobel, F. *J. Phys. Chem. B* **2005**, *109,* 22928-22934.
35. Sauvage, J.-P.; Collin, J.-P.; Chambron, J.-C.; Guillerez, S.; Coudret, C.; Balzani, V.; Barigelletti, F.; De Cola, L.; Flamigni, L. *Chem. Rev.* **1994**, *94,* 993-1019.
36. Baranoff, E.; Collin, J.P.; Flamigni, L.; Sauvage, J.P. *Chemical Society Reviews* **2004**, *33,* 147-155.
37. Juris, A.; Balzani, V.; Barigelletti, F.; Campagna, S.; Belser, P.; Von Zelewsky, A. *Coord. Chem. Rev.* **1988**, *84,* 85-277.
38. Sjodin, M.; Styring, S.; Wolpher, H.; Xu, Y.H.; Sun, L.C.; Hammarstrom, L. *J. Am. Chem. Soc.* **2005**, *127,* 3855-3863.
39. Sjodin, M.; Ghanem, R.; Polivka, T.; Pan, J.; Styring, S.; Sun, L.C.; Sundstrom, V.; Hammarstrom, L. *Phys. Chem. Chem. Phys.* **2004**, *6,* 4851-4858.
40. Sjodin, M.; Styring, S.; Akermark, B.; Sun, L.C.; Hammarstrom, L. *J. Am. Chem. Soc.* **2000**, *122,* 3932-3936.
41. Dempsey, J.L.; Esswein, A.J.; Manke, D.R.; Rosenthal, J.; Soper, J.D.; Nocera, D.G. *Inorg. Chem.* **2005**, *44,* 6879-6892.
42. Konduri, R.; de Tacconi, N.R.; Rajeshwar, K.; MacDonnell, F.M. *J. Am. Chem. Soc.* **2004**, *126,* 11621-11629.

43. Konduri, R.; Ye, H.; MacDonnell, F.M.; Serroni, S.; Campagna, S.; Rajeshwar, K. *Angew. Chem. Int. Ed.* **2002**, *41,* 3185-3187.
44. Barigelletti, F.; Flamigni, L. *Chem. Soc. Rev.* **2000**, *29,* 1-12.
45. Ziessel, R.; Hissler, M.; El-Ghayoury, A.; Harriman, A. *Coord. Chem. Rev.* **1998**, *180,* 1251-1298.
46. Jia, W.L.; Hu, Y.F.; Gao, J.; Wang, S.N. *Dalton Trans.* **2006**, 1721-1728.
47. de Silva, A.P.; Gunaratne, H.Q.N.; Gunnlaugsson, T.; Huxley, A.J.M.; McCoy, C.P.; Rademacher, J.T.; Rice, T.E. *Chem. Rev.* **1997**, *97,* 1515 - 1566.
48. Ashton, P.R.; Ballardini, R.; Balzani, V.; Boyd, S.E.; Credi, A.; Gandolfi, M.T.; GomezLopez, M.; Iqbal, S.; Philp, D.; Preece, J.A.; Prodi, L.; Ricketts, H.G.; Stoddart, J.F.; Tolley, M.S.; Venturi, M.; White, A.J.P.; Williams, D.J. *Chem. Eur. J.* **1997**, *3,* 152-170.
49. Metcalfe, C.; Thomas, J.A. *Chemical Society Reviews* **2003**, *32,* 215-224.
50. Kalyanasundaram, K., *Photochemistry of Polypyridine and Porphyrin Complexes*. 1992, Suffolk: Academic Press.
51. Murov, S.L.; Carmichael, I.; Hug, G.L., *Handbook of photochemistry*. 2 ed. 1993, New York: Marcel Dekker.
52. Pomeranc, D.; Heitz, V.; Chambron, J.-C.; Sauvage, J.-P. *J. Am. Chem. Soc.* **2001**, *123,* 12215-12221.
53. Gilbert, A.; Baggott, J., *Essentials of Molecular Photochemistry*. 1991, Oxford: Blackwell Sciences Ltd.
54. M. Kasha *Discuss. Faraday Soc.* **1950**, *9,* 14.
55. Fermi, E., *Nuclear Physics*. 1950: University of Chicago Press.
56. Englman, R.; Jortner, J. *J. Mol. Phys.* **1970**, *18,* 145.
57. Caspar, J.V.; Kober, E.M.; Sullivan, P.; Meyer, T.J. *J. Am. Chem. Soc.* **1982**, *104,* 630-632.
58. Kober, E.M.; Caspar, J.V.; Lumpkin, R.S.; Meyer, T.J. *J. Phys. Chem.* **1986**, *90,* 3722-3734.
59. Caspar, J.V.; Meyer, T.J. *J. Phys. Chem.* **1983**, *87,* 952-957.
60. Caspar, J.V.; Sullivan, B.P.; Kober, E.M.; Meyer, T.J. *Chem. Phys. Lett.* **1982**, *91,* 91-95.
61. Dexter, D.L. *J. Chem. Phys* **1953**, *21,* 836-850.
62. Förster, T. *Discussions Faraday Soc.* **1959**, *27,* 7-17.
63. Rehm, D.; Weller, A. *Israeli journal of chemistry* **1970**, *8,* 259-271.
64. Meyer, T.J. *Pure Appl. Chem.* **1986**, *58,* 1193-1206.
65. Hager, G.D.; Crosby, G.A. *J. Am. Chem. Soc.* **1975**, *97,* 7031-7037.
66. Hager, G.D.; Watts, R.J.; Crosby, G.A. *J. Am. Chem. Soc.* **1975**, *97,* 7037-7041.
67. Hipps, K.W.; Crosby, G.A. *J. Am. Chem. Soc.* **1975**, *97,* 7042-7048.
68. McCusker, J.K. *Acc. Chem. Res.* **2003**, *36,* 876-887.
69. Bhasikuttan, A.C.; Suzuki, M.; Nakashima, S.; Okada, T. *J. Am. Chem. Soc.* **2002**, *124,* 8398-8405.
70. Allen, G.H.; White, R.P.; Rillema, D.P.; Meyer, T.J. *J. Am. Chem. Soc.* **1984**, *106,* 2613-2620.
71. Rillema, D.P.; Allen, G.; Meyer, T.J.; Conrad, D. *Inorg. Chem.* **1983**, *22,* 1617-1622.

72. Barigelletti, F.; Juris, A.; Balzani, V.; Belser, P.; Zelewsky, A.v. *J. Phys. Chem* **1987**, *91,* 1095-1098.
73. Barigelletti, F.; Juris, A.; Balzani, V.; Belser, P.; Von Zelewsky, A. *Inorg. Chem.* **1983**, *22,* 3335-3339.
74. Brennaman, M.K.; Alstrum-Acevedo, J.H.; Fleming, C.N.; Jang, P.; Meyer, T.J.; Papanikolas, J.M. *J. Am. Chem. Soc.* **2002**, *124,* 15094-15098.
75. Brennaman, M.K.; Meyer, T.J.; Papanikolas, J.M. *J. Phys. Chem. A* **2004**, *108,* 9938-9944.
76. Olofsson, J.; Onfelt, B.; Lincoln, P. *J. Phys. Chem. A* **2004**, *108,* 4391-4398.
77. Onfelt, B.; Olofsson, J.; Lincoln, P.; Norden, B. *J. Phys. Chem. A* **2003**, *107,* 1000-1009.
78. Collin, J.-P.; Guillerez, S.; Sauvage, J.-P.; Barigelletti, F.; De Cola, L.; Flamigni, L.; Balzani, V. *Inorg. Chem.* **1991**, *30,* 4230-4238.
79. Gray, H.B. *Journal of Chemical Education* **1964**, *41,* 2-12.
80. Kettle, S.F.A., *Physical inorganic chemistry. A coordination chemistry approach*. 2000: Oxford University Press.
81. Treadway, J.A.; Loeb, B.; Lopez, R.; Anderson, P.A.; Keene, F.R.; Meyer, T.J. *Inorg. Chem.* **1996**, *35,* 2242-2246.
82. Caspar, J.V.; Meyer, T.J. *Inorg. Chem.* **1983**, *22,* 2444-2453.
83. Hammarström, L.; Barigelletti, F.; Flamigni, L.; Indelli, M.T.; Armaroli, N.; Calogero, G.; Guardigli, M.; Sour, A.; Collin, J.-P.; Sauvage, J.-P. *J. Phys. Chem. A.* **1997**, *101,* 9061-9069.
84. Webb, M.A.; Knorr, F.J.; McHale, J.L. *J. Raman Spec.* **2001**, *32,* 481-485.
85. Wallin, S.; Davidsson, J.; Modin, J.; Hammarstrom, L. *J.Phys. Chem. A* **2005**, *109,* 4697-4704.
86. Kelly, L.A.; Rodgers, M.A.J. *J. Phys. Chem.* **1995**, *99,* 13132-13140.
87. Malone, R.A.; Kelley, D.F. *Journal of Chemical Physics* **1991**, *95,* 8970-8976.
88. Medlycott, E.A.; Hanan, G.S. *Coord. Chem. Rev.* **2006**, *250,* 1763-1782.
89. Medlycott, E.A.; Hanan, G.S. *Chem. Soc. Rev.* **2005**, *34,* 133-142.
90. Duati, M.; Fanni, S.; Vos, J.G. *Inorg. Chem. Commun.* **2000**, *3,* 68-70.
91. Duati, M.; Tasca, S.; Lynch, F.C.; Bohlen, H.; Vos, J.G.; Stagni, S.; Ward, M.D. *Inorg. Chem.* **2003**, *42,* 8377-8384.
92. Constable, E.C.; Cargill Thompson, A.M.W.; Armaroli, N.; Balzani, V.; Maestri, M. *Polyhedron* **1992**, *11,* 2707-2709.
93. Maestri, M.; Armaroli, N.; Balzani, V.; Constable, E.C.; Cargill Thompson, A.M.W. *Inorg. Chem.* **1995**, *34,* 2579-2767.
94. Wang, J.H.; Fang, Y.Q.; Hanan, G.S.; Loiseau, F.; Campagna, S. *Inorg. Chem.* **2005**, *44,* 5-7.
95. Indelli, M.T.; Bignozzi, C.A.; Scandola, F.; Collin, J.P. *Inorg. Chem.* **1998**, *37,* 6084-6089.
96. Son, S.U.; Park, K.H.; Lee, Y.S.; Kim, B.Y.; Choi, C.H.; Lah, M.S.; Jang, Y.H.; Jang, D.J.; Chung, Y.K. *Inorg. Chem.* **2004**, *43,* 6896-6898.
97. Constable, E.C.; Thompson, A.M.W.; Cherryman, J.; Liddiment, T. *Inorg. Chim. Acta* **1995**, *235,* 165-171.

98. Collin, J.P.; Beley, M.; Sauvage, J.P.; Barigelletti, F. *Inorg. Chim. Acta* **1991**, *186,* 91-93.
99. Barigelletti, F.; Ventura, B.; Collin, J.P.; Kayhanian, R.; Gavina, P.; Sauvage, J.P. *Eur. J. Inorg. Chem.* **2000**, 113-119.
100. Beley, M.; Collin, J.P.; Sauvage, J.P. *Inorg. Chem.* **1993**, *32,* 4539-4543.
101. Beley, M.; Collin, J.P.; Louis, R.; Metz, B.; Sauvage, J.P. *J. Am. Chem. Soc.* **1991**, *113,* 8521-8522.
102. Polson, M.I.J.; Loiseau, F.; Campagna, S.; Hanan, G.S. *Chem. Comm.* **2006**, 1301-1303.
103. Polson, M.I.J.; Medlycott, E.A.; Hanan, G.S.; Mikelsons, L.; Taylor, N.L.; Watanabe, M.; Tanaka, Y.; Loiseau, F.; Passalacqua, R.; Campagna, S. *Chem. Eur. J.* **2004**, *10,* 3640-3648.
104. Fang, Y.Q.; Taylor, N.J.; Hanan, G.S.; Loiseau, F.; Passalacqua, R.; Campagna, S.; Nierengarten, H.; Van Dorsselaer, A. *J. Am. Chem. Soc.* **2002**, *124,* 7912-7913.
105. Encinas, S.; Flamigni, L.; Barigelletti, F.; Constable, E.C.; Housecroft, C.E.; Schofield, E.R.; Figgemeier, E.; Fenske, D.; Neuburger, M.; Vos, J.G.; Zehnder, M. *Chem. Eur. J.* **2002**, *8,* 137-150.
106. Ceroni, P.; Credi, A.; Balzani, V.; Campagna, S.; Hanan, G.S.; Arana, C.R.; Lehn, J.M. *Eur. J. Inorg. Chem.* **1999**, 1409-1414.
107. Hissler, M.; El-ghayoury, A.; Harriman, A.; Ziessel, R. *Angew. Chem. Int. Ed.* **1998**, *37,* 1717-1720.
108. Hammarstrom, L.; Barigelletti, F.; Flamigni, L.; Indelli, M.T.; Armaroli, N.; Calogero, G.; Guardigli, M.; Sour, A.; Collin, J.P.; Sauvage, J.P. *J. Phys. Chem. A.* **1997**, *101,* 9061-9069.
109. Fang, Y.-Q.; Taylor, N.J.; Hanan, G.S.; Loiseau, F.; Passalacqua, R.; Campagna, S.; Nierengarten, H.; Van Dorsselaer, A. *J. Am. Chem. Soc.* **2002**, *124*.
110. Wang, X.Y.; Del Guerzo, A.; Schmehl, R.H. *J. Photochem. Photobiol. C* **2004**, *5,* 55-77.
111. Baba, A.I.; Shaw, J.R.; Simon, J.A.; Thummel, R.P.; Schmehl, R.H. *Coord. Chem. Rev.* **1998**, *171,* 43-59.
112. Passalacqua, R.; Loiseau, F.; Campagna, S.; Fang, Y.-Q.; Hanan, G.S. *Angew. Chem. Int. Ed.* **2003**, *42,* 1608-1611.
113. Wang, J.H.; Hanan, G.S.; Loiseau, F.; Campagna, S. *Chem. Comm.* **2004**, 2068-2069.
114. McClenaghan, N.D.; Leydet, Y.; Maubert, B.; Indelli, M.T.; Campagna, S. *Coord. Chem. Rev.* **2005**, *249,* 1336-1350.
115. Hissler, M.; Harriman, A.; Khatyr, A.; Ziessel, R. *Chem. Eur. J.* **1999**, *5,* 3366-3381.
116. Simon, J.A.; Curry, S.L.; Schmehl, R.H.; Schatz, T.R.; Piotrowiak, P.; Jin, X.Q.; Thummel, R.P. *J. Am. Chem. Soc.* **1997**, *119,* 11012-11022.
117. Harriman, A.; Hissler, M.; Khatyr, A.; Ziessel, R. *Chemical Communications* **1999**, 735-736.
118. Ford, W.E.; Rodgers, M.A.J. *J. Phys. Chem.* **1992**, *96,* 2917-2920.
119. Tyson, D.S.; Henbest, K.B.; Bialecki, J.; Castellano, F.N. *J. Phys. Chem. A* **2001**, *105,* 8154-8161.

120. Lashgari, K.; Kritikos, M.; Norrestam, R.; Norrby, T. *Acta Cryst. Sec. C* **1999**, 64-67.
121. Sauvage, J.P.; Collin, J.P.; Chambron, J.C.; Guillerez, S.; Coudret, C.; Balzani, V.; Barigelletti, F.; Decola, L.; Flamigni, L. *Chem. Rev.* **1994**, *94,* 993-1019.
122. Harrigan, R.W.; Crosby, G.A. *J. Chem. Phys.* **1973**, *59,* 3468-3476.
123. Crosby, G.A.; Demas, J.N. *J. Am. Chem. Soc.* **1971**, *93,* 2841-2847.
124. Stone, M.L.; Crosby, G.A. *Chem. Phys. Lett.* **1981**, *79,* 169-173.
125. Caspar, J.V.; Westmoreland, T.D.; Allen, G.H.; Bradley, P.G.; Meyer, T.J.; Woodruff, W.H. *J. Am. Chem. Soc.* **1984**, *106,* 3492-3500.
126. Coe, B.J.; Thompson, D.W.; Culbertson, C.T.; Schoonover, J.R.; Meyer, T.J. *Inorg. Chem.* **1995**, *34,* 3385-3395.
127. Sun, H.; Hoffman, M.Z. *J. Phys. Chem.* **1993**, *97,* 11956-11959.
128. Clark, C.D.; Hoffman, M.Z.; Rillema, D.P.; Mulazzani, Q.G. *J. Photochem. Photobiol. A* **1997**, *110,* 285-290.
129. Lomoth, R.; Haupl, T.; Johansson, O.; Hammarstrom, L. *Chem. Eur. J.* **2002**, *8,* 102-110.

Acta Universitatis Upsaliensis

Digital Comprehensive Summaries of Uppsala Dissertations from the Faculty of Science and Technology 237

Editor: The Dean of the Faculty of Science and Technology

A doctoral dissertation from the Faculty of Science and Technology, Uppsala University, is usually a summary of a number of papers. A few copies of the complete dissertation are kept at major Swedish research libraries, while the summary alone is distributed internationally through the series Digital Comprehensive Summaries of Uppsala Dissertations from the Faculty of Science and Technology. (Prior to January, 2005, the series was published under the title "Comprehensive Summaries of Uppsala Dissertations from the Faculty of Science and Technology".)

Distribution: publications.uu.se
urn:nbn:se:uu:diva-7230

ACTA
UNIVERSITATIS
UPSALIENSIS
UPPSALA
2006